

Magnetism in the strained ordered phases of $\text{Pt}_x\text{Fe}_{1-x}$ and $\text{Pt}_x\text{Co}_{1-x}$ ($x=0.25, 0.5,$ and 0.75)

I. G. Shuttleworth,
School of Science and Technology,
Nottingham Trent University,
Nottingham NG11 8NS.
UK

E-mail: ian.shuttleworth@ntu.ac.uk

Abstract

The response of the magnetic moment of the $L1_0$ and $L1_2$ ordered phases of $\text{Pt}_x\text{M}_{1-x}$ ($\text{M}=\text{Fe},\text{Co}$) ($x=0.25, 0.5,$ and 0.75) to compressive and tensile strains have been investigated using density functional theory (DFT). The magnetic moment of the $\text{Pt}_{0.75}\text{M}_{0.25}$ and $\text{Pt}_{0.50}\text{M}_{0.50}$ phases varies linearly compared to the response of the $\text{Pt}_{0.25}\text{M}_{0.75}$ alloys which shows a transition in the rate of change of magnetic moment at approximately zero strain. For all phases the mechanism of magnetic moment change under strain is shown to be intra-orbital charge transfer within the Pt, Fe and Co d shells. The strained and equilibrium magnetic band structures of each phase contain spin-orbit effects which are presented and discussed.

1. Introduction

Magnetovolume effects are conventionally used to describe the deformation of a magnetic sample during changes in its magnetic moment. Studies within this field have sought to investigate the dependence between magnetic deformations and changes to the crystalline structure which can be induced, for example, by applying pressure to the sample. These investigations have been performed across a large range of materials including MnGe [1], BiMnO₃ [2] and La(Fe_xSi_{1-x})₁₃ [3] as well as for Invar alloys [4] which showed a quenching of magnetic moment under applied pressures [5]. The current work will investigate the interdependence of magnetic moment and lattice stress for a group of ordered transition metal alloys composed of either Pt-Fe or Pt-Co.

a. Pt-Fe alloys

FePt-Fe₃Pt nanocomposites are of significant technological importance as potential permanent magnetic materials as they have a large energy product (the combination of permanent magnetic field and magnetic moment) compare to single phase materials [6]. The stability of pure Fe, Co and Ni under high pressures has been investigated theoretically [7] and has shown that the ferromagnetic state of the material is very sensitive to structure as well as the applied pressure. Comparative studies have been performed on the related Fe_xNi_{1-x} alloys. These alloys contain two strongly magnetic components rather than a single strongly magnetic component and the weaker Pt component of the current study. However, the behaviour of both sets of alloys might be anticipated to be similar as both form substitutional alloys. High pressure experimental studies [8] of the Fe₆₄Ni₃₆ and Fe-Pt Invar alloys have shown that the magnetic moment of the materials evolve as the pressure increases. The effect of torsional deformation under pressure on alloys close to the stoichiometric Pt₃Fe [9] has been shown to transform the alloy from an anti-ferromagnetic state ($T_N = 164$ K) into the ferromagnetic state ($T_C \sim 400$ K). The temperature-dependent effects of pressure have also been seen in studies of the Curie temperature of Fe₃Pt [10-11]. Studies have also been performed on the acquisition of magnetic remanence of iron-nickel alloys (Fe₆₄Ni₃₆, Fe₅₈Ni₄₂, and Fe₅₀Ni₅₀) and pure Ni under pressures up to 23 GPa [12]. In these studies strain may accumulate irreversibly throughout the system. The studies demonstrated a correlation between materials that exhibit high magnetostriction and the rate of acquisition of magnetic remanence.

The magnetism of disordered FePt has been investigated using the coherent potential approximation (CPA) [13] and a sequence of special quasirandom structures. The studies have shown that magnetic moments of the Fe atoms are more robust to local changes in the environment than the Pt atoms. The studies also showed that the magnetic moments of the Fe atoms increases as the average Fe-Fe distance is increased, and that the moment of the Pt atoms decreases as the average Fe-Pt distance increases. The importance of short range order were highlighted in earlier studies [14] of the Invar anomalies of Fe-Ni, Fe-Ni-Co and Fe-Pt alloy. The work demonstrated that the negative anharmonicity of the crystal lattices were due to the consequent tendency of the alloys to have a smaller lattice constant. First-principles calculations of the lattice constants of the ordered L1₀ and L1₂ phases of PtFe₃, PtFe and Pt₃Fe [15] have shown a non-linear compositional dependence and this dependence is also shared in the changes to the total magnetic moments. The disordered local moment (DLM) technique has been applied to disordered Fe-Pt alloys [16] and has shown that the reduction of the local magnetic moments gives rise to the experimentally observed anomaly in the temperature

dependence of the magnetic moment. Studies have also shown [17] that the orientation of the magnetic moments in FePt alloys is more predominantly more sensitive to chemical disorder than lattice distortion though studies of the group of TX ordered alloys (T=Fe,Co and X=Pd,Pt) [18] have interpreted the magnetocrystalline anisotropy energy (MAE) in terms of interatomic interactions in the crystal. Early experimental studies of platinum/iron alloys with composition close to Pt₃Fe [19] have shown that the magnetic structure is determined particularly by the nearest neighbour Fe atoms and the chemical order of the sample. To summarise, these studies shown that magnetic state of the component atoms of an Fe-Pt alloy are significant in determining the mechanical properties of the alloy and conversely that the orientational dependence of the magnetic components of these systems is closely linked to the structure. However, no general trend has currently arisen and so the current work will comparatively study systems with a range of structures and stoichiometries.

Numerous studies have investigated the band structures of Pt-based alloys. In the current work focus will be placed on those that have investigated the role of the electronic structure in determining the magnetic properties of the system [20]. Analysis of the electronic structures of PtFe₃, PtFe, Pt₃Fe and Pt₅Fe₃ [21] reiterated the model that Invar materials are composed of two nearly degenerate states at 0K: a high-spin (HS) state with large volume, and a low-spin (LS) state with a smaller volume. The low spin state may be non-magnetic though this is not a prerequisite. Consequently the metric for determining the equation of state for the systems investigated in the current study will focus on the system energy and magnetic moment rather than on the lattice dimensions. For PtFe₃ [22] a pressure dependence on the total energy of the system and the sensitivity of the HS and LS branches on this pressure dependency was identified and discussed. However the work also indicated limitations of the local density approximation (LDA) to model these dependencies accurately.

Early tight binding calculations of ordered TPt (T = Ti, V, Cr, Mn, Fe and Co) alloys [23] predicted that the most stable FePt₃ alloys carried no magnetic moment on the Pt atoms. Studies of the disordered and ordered Fe₃Pt alloys [24] showed that Fe and Pt carry moments of approximately 2.8 and 0.3 μ_B , respectively. The significance of the finite magnetic moment of the Pt atoms is seen more fully in investigations of the optical properties of these alloys. Technologically these properties are critical, particularly in the use of these alloys in recording media [25] and in fundamental of studies of e.g. optical conductivity [26] and band splitting [27] that support these applications. Calculations of ordered and disordered Fe₃Pt [28] presented localized magnetic moments for Fe of (2.03 \pm 0.02 μ_B) and Pt (0.34 \pm 0.08 μ_B). The magnetic properties of the alloys found to be fairly robust against using different calculational methods and against choosing the ordered and disordered phases. These conclusions highly suggestive that studies of the magnetic properties of ordered phases of these systems may be equivalent to the magnetic properties of disordered phases and consequently a range of ordered phases will be investigated in the current work.

b. Pt-Co alloys

Comparative studies of the Fe–Pt and Co–Pt disordered alloys [29] have shown that these systems tend to order and have underscored the comparative nature of these alloy systems. The spin moment of the Co (Pt) atoms in CoPt₃ [30] were estimated to be 1.88 μ_B (0.17 μ_B) using scalar-relativistic LAPW calculations. The values compare to the spin moments of the Fe (Pt) atoms in FePt₃ [30] which were estimated to be 3.10 μ_B (0.20 μ_B) in the same study. Statistical and experimental studies [31] also demonstrated the sensitivity of the Pt moment on its local

environment on $\text{Co}_x\text{Pt}_{1-x}$. The technological importance of the platinum/cobalt alloys, particularly the $L1_0$ ordered CoPt alloy, is due to their large magnetocrystalline anisotropy energy (MAE) which potentially be used in room-temperature memory bits [32] though the production of this phase has been seen to depend sensitively on annealing temperature [33]. Thermal effects have been shown not to be unique in their effects on the ordering of Co-Pt alloys. In a comparative study [34] the degree of order in CoPt and the magnetism of the sample were shown to be mutually sustaining as the ordering of the equiatomic CoPt alloy into an $L1_0$ structure was shown to favour strong magnetic anisotropy; in turn, it was then shown that magnetism can re-inforce the chemical ordering of the system.

Contemporary attempts to tune the properties of Co-Pt alloys have also focussed on nanoparticle growth through their size and composition. In studies of the $\text{Co}_n\text{Pt}_{M-n}$ ($M=13, 19, 55$) [35] and $\text{Co}_{n-x}\text{Pt}_x$ ($n=2-13, 38, 55$) [36] nanoparticles the Pt atoms tended to segregate to the surface of the nanoparticle; this is common phenomena in nanoparticle technology and can often be exploited to control the size of reactive centres [37]. Further complexity is introduced when supports are added to the nanoclusters and both CoPt and FePt are widely exploited materials in this field [38] because of the delicate interplay between their structural, magnetic and electronic characters.

The current work will investigate the ordered $L1_0$ and $L1_2$ phases of Pt_3M , PtM and PtM_3 ($M=\text{Fe,Co}$) using both scalar and vector relativistic density functional theory (DFT). The work will focus on changes to the magnetic moment of the bulk phases of these alloys at equilibrium (strain $\epsilon=0\%$) and also under both compressive and tensile. The work will also provide an overview of the magnetic band structures of these alloys under the same conditions and highlight the importance of the spin-orbit correction (SOC) to these studies. The work is structured in the following way: in Section 2 the Computational Details are presented, and then in Sections 3 (a) and (b) the results from investigations of the Pt-Fe and Pt-Co alloys, respectively, are presented before the key findings are summarised in the Section 4 Conclusions.

2. Computational Details

The Quantum Espresso package [39] was used to perform the plane-wave density functional theory (DFT) simulations presented in this work. Scalar and vector relativistic ultra-soft pseudopotentials with non-linear core corrections were used [40-41] together with a wave-function kinetic energy cut-off of 75 Ry and a charge density/potential cut-off of 900 Ry. These cut-off's provided convergence of the magnetic moments, density of states, spin polarisations and geometric c/a ratio (where relevant) which were analysed in the subsequent sections of this work. Vector (scalar) relativistic pseudopotentials were used exclusively for the non-collinear (collinear) simulations and both collinear and non-collinear spin-polarised simulations were performed in the current work. A Brillouin zone sampling of $(20 \times 20 \times 20)$ was used for all the results presented in this work though trials indicated that convergence could be approached with sampling between $(12 \times 12 \times 12)$ and $(14 \times 14 \times 14)$. Brillouin zone sampling was performed using a first-order Methfessel-Paxton smearing of 0.02 Ry [42]. The magnetic lowest energy state was determined during each non-collinear simulation by stepping the polar and azimuthal angles in increments of $\pi/4$ through ranges of $[0, 2\pi]$ and starting the simulation for each initial orientation.

Fig. 1 shows the structures of the $L1_0$ and $L1_2$ ordered phases of the Pt-Fe and Pt-Co alloys. Lattice strain ε was defined as

$$\varepsilon = \left(\frac{a_s - a}{a} \right) \times 100\% \quad (1)$$

The strained and equilibrium (zero strain) lattice constants are a_s and a , respectively. For the $L1_0$ simulations the ratio c/a was not changed during strain as the strain was hydrostatic. The strained and equilibrium $[001]$ lattice constants, c_s and c respectively, were related by

$$\frac{c_s}{a_s} = \frac{c}{a} \quad (2)$$

Table 1 summarises the structural parameters determined for these systems. The structural parameters presented in Table 1 were compared with parameters obtained from simulations using a wave-function kinetic energy cut-off and a charge density/potential kinetic energy cut-off of 100 Ry and 1200 Ry, respectively. No significant differences were observed indicating that convergence had been achieved. The results in Table 1 indicate that agreement between the computational structural parameters presented in the current work and the experimental values improves when semi-core states are included in the DFT simulations. This agreement generally continued with the inclusion of an f semi-core state to the Pt pseudopotential.

3. Results and Discussion

a. Pt-Fe alloys

Fig. 2 shows the variation of the Pt and Fe contributions to the magnetic moment μ with strain ε for each Pt-Fe alloy and for both non-collinear and collinear simulations. The contributions from the s, p and f states to the magnetic moment for both elements were zero for all strains. The curves show that the variation of μ with ε is approximately linear for the Pt and Fe contributions for Pt₃Fe and PtFe alloys. This compares with the behaviour of both the Pt and the Fe contributions for the PtFe₃ alloy. Under most compressive strains the rate of change of μ for the Fe d contributions is greater than the rate of change of μ for tensile strains. This change produces the non-linearity seen in Fig. 2 (a). A similar transition in the rate of change of μ is seen in Fig. 2 (b) for the Pt d contributions though in this case the transition is shifted towards the tensile stress region of the graph.

A correlation exists between the strain-induced changes in μ for the non-collinear and collinear cases. This can be seen in Fig. 2 (a) for the Fe d states where, for the Pt₃Fe and PtFe alloys, the rate of change of μ is comparable for both the non-collinear and collinear simulations. An offset exists between the non-collinear and collinear curves. This indicates that an additional constant, strain independent interaction exists between the collinear or the non-collinear models but that the response of either model to strain is at least qualitatively the same. A similar though less distinct relationship exists for the PtFe₃ alloy which is also shown in fig. 2.

Changes in μ for both the non-collinear and collinear states should arise from changes in the charge distribution. The susceptibility of the alloy to this change will be greater if it carries a larger moment which is the case for the Fe₃Pt alloy when compared to the FePt₃ alloy. The reason for this larger moment is because of the greater concentration of highly magnetic carriers (Fe) over the less magnetic Pt components. A similar effect is seen for the Co-containing alloys presented later in the current work. A population analysis of the Pt and Fe states was performed to investigate these changes. The analysis was performed for each simulation set, where the pseudopotentials had no semi-core states and when the pseudopotentials had either sp (Pt,Fe) or spf (Pt) semi-core states. In all cases the conclusions drawn from the analysis were qualitatively and, to a large extent quantitatively, the same. Because of this an oversight of the analysis will be presented here and the full analysis is presented in Supplementary Table S1.

The fractional change in the occupation of each of the s, p and d states for the Pt and Fe species are typically a few per cent or much less under strains $\varepsilon=\pm 5\%$ when compared to their occupation at equilibrium $\varepsilon=0\%$. This trend is seen for each of the stoichiometries considered in the current work. Fractional changes to the d states are typically greater than those of the s states, and the changes to the p states are minor. This analysis shows that during strain a fractionally small amount of charge is transferred between the s, p and d states of the Pt and Fe atoms. These fractional amounts of charge exchange are insufficient to generate that change in the magnetic moment presented in Fig. 2. Consequently, a more refined analysis is necessary to identify the origin of the changes in magnetic moment.

To enable this analysis the projected density of states (PDOS) curves for each alloy were analysed by calculating the occupancy

$$N_{d,j,m_j}^M(\varepsilon) = \int_{E=-\infty}^{E_F} n_{d,j,m_j}^M(\varepsilon, E) dE \quad (3)$$

M is either Fe, Co or Pt and $n_{d,j,m_j}^M(\varepsilon, E)$ is the energy-resolved projected density of states for d orbitals with total angular momentum j and components m_j using the conventional non-collinear notation. The energy-resolved total projected density of states (PDOS) curves and the j-resolved curves $\sum_{m_j} n_{d,j,m_j}^M(\varepsilon = 0\%, E)$ for unstrained Pt₃Fe, PtFe, and PtFe₃, are shown in

Supplementary Figure Fig. S1. The total occupancy of each j-state is

$$N_{d,j}^M(\varepsilon) = \sum_{m_j} N_{d,j,m_j}^M(\varepsilon) \quad (4)$$

Table 2 shows the total occupancies $N_{d,j}^M(\varepsilon)$ for each of the Pt-Fe alloys at equilibrium ($\varepsilon=0\%$).

The fractional change of $N_{d,j}^M(\varepsilon)$ at a particular strain ε was calculated using

$$\delta N_{d,j}^M(\varepsilon) = \frac{N_{d,j}^M(\varepsilon) - N_{d,j}^M(0)}{N_{d,j}^M(0)} \times 100\% \quad (5)$$

The values of $\delta N_{d,j}^M(\varepsilon)$ presented in Table 2 have magnitudes of less than 2% which correspond to fractional changes in occupation of each j-orbital. This amount is again small when compared to the changes in magnetic moment presented in Fig. 2. To identify to amount of intra-orbital charge transfer that occurs during strain the variance of $N_{d,j,m_j}^M(\varepsilon)$, which is related to the occupancy of individual m_j orbitals, was calculated

$$v = v(M, j, \varepsilon) = \text{Var}(N_{d,j,m_j}^M(\varepsilon)) \quad (6)$$

The v are presented in Fig. 3 for each of the Pt-Fe alloys. The largest variation in v is seen for the Fe d j=2.5 states and then the Fe d j=1.5. Fe is the most magnetic of species in each alloy and its magnetic moment is the most susceptible to strain. Further susceptibility is attracted by the higher angular momentum states of this metal. For the Pt₃Fe alloy v changes by approximately 20% across the range of values presented in Fig. 3 (a) for the Fe d j=2.5 state, and by over 50% for the PtFe₃ alloy, Fig. 3 (c). These changes in v during strain are clearly

much larger than the fractional changes in $\delta N_{d,j}^M(\epsilon)$ presented in Table 2 and the changes in the total shell occupancies discussed earlier in this section and presented in Supplementary Table S1. The predominant mechanism of charge transfer during strain of the Pt-Fe alloys is therefore intra-orbital transfer between the m_j states. This charge transfer gives rise to the changes in the magnetic moment of the Pt-Fe alloys presented in Fig. 2 and indicates that inter-atom or inter-orbital hopping mechanisms do not give rise to changes in the magnetic moment of these alloys under strain.

To further elucidate the charge transfer within the d-orbitals during strain the normalised variance of $N_{d,j,m_j}^M(\epsilon)$ was calculated using

$$v_{\text{norm}} = v_{\text{norm}}(M, j, \epsilon) = \frac{v(M, j, \epsilon)}{\sum_j v(M, j, \epsilon)} \quad (7)$$

The v_{norm} for the strained Pt-Fe alloys are shown in Fig. 4. For each alloy changes in v_{norm} with strain are relatively small for the Fe states. For the Pt states the v_{norm} for the Pt d $j=1.5$ and Pt d $j=2.5$ are correlated with one another – this can be seen most clearly in Fig. 4 (c) where increases in v_{norm} for the Pt d $j=2.5$ state are mirrored by decreases in v_{norm} for the Pt d $j=1.5$ state. This behaviour is seen to a lesser extent for the Pt₃Fe alloy curves presented in Fig. 4 (a) though is much less pronounced for the PtFe curves in Fig. 4 (b). This analysis suggests that the changes to the distribution of charge within the m_j states of the Pt atoms are not correlated between groups of m_j states in either the Pt d $j=1.5$ and Pt d $j=2.5$ orbitals whereas a much higher degree of correlation is seen between states in Fe atoms. This effect is more prevalent for the L1₂ alloys, particularly the PtFe₃ which has a comparatively high Fe concentration. Non-local interactions between atoms are proposed as the mechanism for this loss of correlation between the Pt states as direct hopping-mediated interactions have been shown earlier in this section to be relatively minor, though the precise dependence of these interactions on stoichiometry and structures is not clear.

Fig. 5 shows the magnetic band structures for the Pt-Fe alloys at equilibrium ($\epsilon=0\%$) and under strain ($\epsilon=\pm 5\%$). The band structures presented in Fig. 5 were calculated using non-collinear spin polarisation. The total spin polarisation $S(\mathbf{k}, E)$ was defined as

$$S(\mathbf{k}, E) = \sqrt{S_1^2(\mathbf{k}, E) + S_2^2(\mathbf{k}, E) + S_3^2(\mathbf{k}, E)} \quad (8)$$

S_1 , S_2 , and S_3 are the expectation values of the σ_1 , σ_2 and σ_3 Pauli spin operators, respectively.

The band structures in Fig. 5 narrow as the strain becomes increasingly tensile for each Pt-Fe alloy. The band structures are composed of a mixture of weakly and more strongly magnetised bands and the magnetic moment is clearly delocalised with little evidence of local centres of high or low magnetism. Mixing of weakly and more strongly magnetised bands is seen for the

unstrained alloys between $E-E_F \approx -6\text{eV}$ up to the Fermi level. This mixing is seen for each alloy though the range changes as strain is applied. Beneath these levels more strongly magnetised bands appear.

In general the S_1 and S_3 (S_2) were zero and $S_k(k)$ was defined by S_2 (S_3) in the $L1_2$ ($L1_0$) structures. However, some evidence of directionality was identified in the occupied states of the unstrained band structures. For the $L1_2$ structures $S_1 = S_3 \neq 0$ along the ΓR direction [43] and $S_1 \neq 0$ along the ΓM direction. For the $L1_0$ structure, $S_1 = S_2 \neq 0$ along the ΓA direction and $S_1 \neq 0$ ($S_2 \neq 0$) along the ΓR (XA) directions. Differences between the magnetic moment of these alloys have already been demonstrated earlier in this section in discussion of Fig. 2 where it was shown that the variation of μ with ϵ was at least qualitatively the same for both collinear and non-collinear simulations. In the current analysis the non-collinear simulation has been seen to demonstrate directionality which has been included by using the spin-orbit correction (SOC). The SOC may be considered to be approximately constant under strain as the changes in μ from both non-collinear and collinear simulations were shown to be at least qualitatively the same in Fig. 2. The directional components discussed here may explain the offsetting between the non-collinear and collinear curves seen in Fig. 2.

b. Pt-Co alloys

Fig. 6 shows the variation of the Pt and Co contributions to the magnetic moment μ with strain ϵ for each Pt-Co alloy and for both non-collinear and collinear simulations. The contributions from the s, p and f states to the magnetic moment for both elements were zero for all strains. The behaviour of the Co d states in Fig. 6 (a) may be compared with that of the Fe d states presented in Fig. 2 (a). The magnetic moment of the Co states at zero strain ($1.8\text{-}2.0\mu_B$) is lower than that for the Fe d states ($2.5\text{-}3.2\mu_B$). There are less quantitative differences between the non-collinear and collinear curves in the Co d curves of Fig. 6 (a) than in between the Fe d curves of Fig. 2 (a). Most notably, the PtCo_3 curves of Fig. 6 (a) agree far more than the PtFe_3 curves of Fig. 2 (a). These changes are not mirrored in the behaviour of the magnetically weaker Pt atom. The offsets and degree of correlation between the non-collinear and collinear curves in Fig. 6 (b) are comparable with those seen in Fig. 2 (b). The importance of non-collinearity is consequently a simple function of the magnetic strength of the atom but depends more subtly on this and both the stoichiometry and the structure of the alloy.

A full population analysis of the Pt and Co s, p and d states was performed and is presented in Supplementary Table S2. The analysis closely mirrors that performed earlier in this current work for the Pt-Fe alloys and shows nominal charge transfers between these states under strain. The total occupancies $N_{d,j}^M(\epsilon)$ for each of the Pt-Co alloys at equilibrium and their fractional changes under strain $\delta N_{d,j}^M(\epsilon)$ presented in Table 2. The $\delta N_{d,j}^M(\epsilon)$ have magnitudes of less than 2% which suggest that the magnetic moment changes seen in Fig. 6 are due to intra-orbital exchange between the m_j states rather than by an inter-orbital or inter-atom mechanism.

The intra-orbital mechanism is explored in Fig. 7 which shows the variance v of the $N_{d,j}^M(\epsilon)$. The energy-resolved total projected density of states (PDOS) curves and the j -resolved curves $\sum_{m_j} n_{d,j,m_j}^M(\epsilon = 0\%, E)$ for unstrained Pt₃Co, PtCo, and PtCo₃, are shown in Supplementary

Figure Fig. S1. This parameter shows a similar trend to those seen for the Pt-Fe alloys in Fig. 3. For each stoichiometry Fig. 7 shows that the variance of the Co d states is greater than that of the Pt atoms with greater variance seen for the higher angular momentum states. These similarities shows that the strain-induced redistribution of charge amongst the m_j states is qualitatively the same between the Pt-Co and Pt-Fe alloys. However the magnitudes of these redistributions are different and are lower for the Pt-Co alloys.

Fig. 8 shows the normalised variance v_{norm} for the Pt-Co alloys. Comparing these quantities with those presented in Fig. 4 for the Pt-Fe alloys it can be seen that, similar to the behaviour of the variance v , the normalised variance v_{norm} for the Pt-Co alloys behaves qualitatively the same as the v_{norm} for the Pt-Fe alloys. The Pt $d_{j=2.5}$ v_{norm} increases for each alloy as the strain becomes increasingly tensile and these increases are mirrored by decreases in the Pt $d_{j=1.5}$ v_{norm} . The magnitude of these changes are smaller for the Pt-Co alloys than for the Pt-Fe alloys indicating that strain-induced loss of correlation between the Pt $d_{j=1.5}$ and Pt $d_{j=2.5}$ states is less for the Pt-Co alloys. Consequently, the variance v and the normalised variance v_{norm} for the Pt-Fe and Pt-Co alloys have been seen to behave qualitatively the same; however, the magnitudes of changes in both quantities are consistently larger for the Pt-Fe alloys.

Fig. 9 shows the magnetic band structures for the Pt-Co alloys at equilibrium ($\epsilon=0\%$) and under strain ($\epsilon=\pm 5\%$). The band structures contain mixtures of weakly and more strongly magnetised bands up to the Fermi level and narrow as ϵ becomes increasingly tensile. Similarly to the Pt-Fe alloy band structures presented in Fig. 5 the S_1 and S_2 were generally zero and $S_k(k)$ was defined by S_3 . However for the L_{12} structures $S_1 = S_2 \neq 0$ for the occupied states along the ΓR direction. In addition, for the L_{10} structures $S_1 = S_2 \neq 0$ for the occupied states along the ΓA direction, and $S_1 \neq 0 (S_2 \neq 0)$ for the occupied states along the ΓR (XA) directions. These directional alignments are very similar to those seen for the Pt-Fe alloys and indicate that for both alloys the spin-orbit correction (SOC) produces a directional magnetic component that is approximately constant under strain.

4. Conclusions

The current work has investigated the ordered L1₀ and L1₂ phases of Pt_xFe_{1-x} and Pt_xCo_{1-x} ($x=0.25, 0.5, \text{ and } 0.75$) using density functional theory (DFT). In particular, the magnetic character of these bulk alloys has been analysed both when the alloys are in a state of either compressive or tensile strain and when the alloys are in equilibrium (strain $\epsilon=0\%$).

The magnetic moment of the alloys has been shown to be entirely due to moments associated with the Pt, Fe and Co d states for crystals under strain and at equilibrium, with no moment associated with the s, p and f states. Strain induces a change in the magnetic moment of each alloy and in general the Co and Fe contribution to the total magnetic moment increases as the strain becomes increasingly tensile for these alloys. Changes in the magnetic moment of these systems has been shown to be due to intra-orbital charge transfer. Stoichiometric factors have also been seen to play an important role in determining the response of the magnetic moment to strain. For the PtM₃ (M=Fe,Co) alloys the increases in the magnetic moment are much greater when the crystals are under compressive strain than when they are under tensile strain. Consequently the variation of magnetic moment with strain is non-linear when compared to variation for the Pt₃M and PtM (M=Fe,Co) alloys.

The magnetic band structures of the strained and equilibrium alloys have been presented and discussed. For both the Pt-Fe and Pt-Co alloys the weakly and more strongly magnetic bands are intermixed between energies of $E-E_F \approx -6\text{eV}$ up to the Fermi level with more strongly magnetic states lying at lower energies. This relation has been seen for both the L1₀ and the L1₂ alloys. In all cases the band structures have narrowed as the strain has become increasingly tensile. An analysis of the occupied non-collinear magnetic states has shown that spin-orbit coupling causes alignment of the magnetic moments with the crystalline structure; this alignment is evident along the ΓA , XA and ΓR directions of the L1₀ alloy for both the Pt-Fe and Pt-Co alloys, along the ΓR direction of the L1₂ alloys and additionally along the ΓM direction for the L1₂ Pt-Fe alloys. These observations have highlighted the importance of including the spin-orbit correction in studies of these alloys.

Acknowledgements

This work was supported by the computational resources of the Supercomputing Laboratory at the King Abdullah University of Science and Technology (KAUST) and by the author's membership of the UK's HEC Materials Chemistry Consortium, which is funded by the EPSRC (EP/L000202) and used the ARCHER UK National Supercomputing Service (<http://www.archer.ac.uk>).

References

- [1] N. Martin, M. Deutsch, J.-P. Itié, J.-P. Rueff, U. K. Rössler, K. Koepernik, L. N. Fomicheva, A. V. Tsvyashchenko, and I. Mirebeau. Magnetovolume effect, macroscopic hysteresis, and moment collapse in the paramagnetic state of cubic MnGe under pressure. *Phys. Rev. B: Condens. Matter* **93(21)** (2016) 214404.
- [2] J. M. Chen, S. C. Haw, J. M. Lee, S. A. Chen, K. T. Lu, S. W. Chen, M. J. Deng, Y.-F. Liao, J. M. Lin, B. H. Chen, F. C. Chou, N. Hiraoka, H. Ishii, K. D. Tsuei, and E. Huang. Pressure-dependent electronic structures and orbital hybridization of Mn 3d states in multiferroic BiMnO₃: A combined x-ray absorption, x-ray emission, and resonant x-ray emission study. *Phys. Rev. B: Condens. Matter* **86(4)** (2012) 045103.
- [3] A. Fujita, K. Fukamichi, J.-T. Wang, and Y. Kawazoe. Large magnetovolume effects and band structure of itinerant-electron metamagnetic La(Fe_xSi_{1-x})₁₃ compounds. *Phys. Rev. B: Condens. Matter* **68(10)** (2003) 1044311-1044316.
- [4] M. van Schilfgaarde, I. A. Abrikosov, and B. Johansson. Origin of the Invar effect in iron–nickel alloys. *Nature* **400** (1999) 46-49.
- [5] J.P. Rueff, A. Shukla, A. Kaprolat, M. Krisch, M. Lorenzen, F. Sette, and R. Verbeni. Magnetism of Invar alloys under pressure examined by inelastic x-ray scattering. *Phys. Rev. B: Condens. Matter* **63(13)** (2001) 1324091-1324094.
- [6] H. Zeng, J. Li, J. P. Liu, Z. L. Wang, and S. Sun. Exchange-coupled nanocomposite magnets by nanoparticle self-assembly. *Nature* **420 (6914)** (2002) 395-398.
- [7] Y. Shoaib Mohammed, Y. Yan, H. Wang, K. Li, and X. Du. Stability of Ferromagnetism in Fe, Co, and Ni Metals under High Pressure with GGA and GGA+U. *J. Magn. Magn. Mater.* **322(6)** (2010) 653-657.
- [8] L. Nataf, F. Decremps, J. C. Chervin, O. Mathon, S. Pascarelli, J. Kamarád, F. Baudelet, A. Congeduti, and J. P. Itié. High-pressure magnetic study of Fe-Ni and Fe-Pt Invar alloys. *Phys. Rev. B: Condens. Matter* **80(13)** (2009) 134404.
- [9] N. I. Kourov, Yu. V. Knyazev, A. V. Korolev, V. G. Pushin, and Yu. A. Dorofeev. Effect of Severe Plastic Deformation on the Properties of the Pt₃Fe Antiferromagnet. *Phys. Solid State* **52(2)** (2010) 317–322.

- [10] G. Oomi, and H. Araki. Effect of pressure on the Curie temperature of Fe₃Pt alloys having different degree of order. *J. Magn. Magn. Mater.* **140-144** (1995) 83-84.
- [11] A. Kashyap, A. K. Solanki, T. Nautiyal, and S. Auluck. Effect of pressure on the Curie temperature of Fe₃Pt. *Phys. Rev. B: Condens. Matter* **52(18)** (1995) 13471-13474.
- [12] Q. Wei, S. A. Gilder, and B. Maier. Pressure dependence on the remanent magnetization of Fe-Ni alloys and Ni metal. *Phys. Rev. B: Condens. Matter* **90(14)** (2014) 144425.
- [13] S. A. Khan, J. Minár, H. Ebert, P. Blaha, and O. Šipr. Local environment effects in the magnetic properties and electronic structure of disordered FePt. *Phys. Rev. B: Condens. Matter* **95** (2017) 014408.
- [14] P. Entel, H. Ebert, V. Crisan, and H. Akai. First-principles calculations of the instabilities in Fe-(Ni, Co, Pt) alloys. *Phase Transitions* **75(1-2)** (2002) 195-200.
- [15] N. Zotov, and A. Ludwig. First-principles calculations of the elastic constants of Fe-Pt alloys. *Intermetallics* **16** (2008) 113-118.
- [16] S. Khmelevskiy, I. Turek, and P. Mohn. Large Negative Magnetic Contribution to the Thermal Expansion in Iron-Platinum Alloys: .Quantitative Theory of the Invar Effect. *Phys. Rev. Lett.* **91(3)** (2003) 037201.
- [17] C. J. Aas, L. Szunyogh, J. S. Chen, and R. W. Chantrell. Magnetic anisotropy of FePt: Effect of lattice distortion and chemical disorder. *Appl. Phys. Lett.* **99** (2011) 132501.
- [18] I. V. Solovyev, P. H. Dederichs, and I. Mertig. Origin of orbital magnetization and magnetocrystalline anisotropy in TX ordered alloys (where T=Fe,Co and X=Pt,Pd). *Phys. Rev. B: Condens. Matter* **52(18)** (1995) 13419-13428.
- [19] G. E. Bacon, and J. Crangle. Chemical and Magnetic Order in Platinum-Rich Pt+Fe Alloys. *Proc. R. Soc. London, Ser. A* **272** (1963) 387-405.
- [20] J. B. Staunton. The electronic structure of magnetic transition metallic materials. *Rep. Prog. Phys.* **57(12)** (1994) 1289-1344.

- [21] M. Podgórný. Electronic structure of the ordered phases of Pt-Fe alloys. *Phys. Rev. B: Condens. Matter* **43(13)** (1991) 11300-11318.
- [22] M. Podgórný. Magnetic instabilities in PtFe₃ and in the fcc Ni-Fe system. *Phys. Rev. B: Condens. Matter* **46(10)** (1992) 6293-6302.
- [23] T. Tohyama, Y. Ohta, and M. Shimizu. Tight-binding calculations of the electronic structure and magnetic properties in ordered TPt₃ (T = Ti, V, Cr, Mn, Fe and Co) alloys. *J. Phys.: Condens. Matter*. **1** (1989) 1789-1798.
- [24] J. Inoue, and M. Shimizu. A calculation of magnetic properties of Fe₃Pt alloys. *J. Phys. F: Met. Phys.* **13** (1983) 2677-2684.
- [25] Z. H. Cen, B. X. Xu, J. F. Hu, L. G. Ng, J. Shanmugam, Y. T. Toh, J. M. Li, K. D. Ye and J. Zhang. Optical properties of L1₀ FePt nanoparticles dispersed in a C matrix. *J. Phys. D: Appl. Phys.* **47** (2014) 445302.
- [26] N. I. Kulikov, E. T. Kulatov, and S. I. Yakhimovich. Theory of antiferromagnetic ordering in Pt₃Fe alloys. I: Self-consistent band-structure calculation. *J. Phys. F: Met. Phys.* **15** (1985) 1127-1 137.
- [27] A. Hasegawa. Spin-Polarised Energy Bands for MnPt₃, FePd₃ and PtFe₃. *J. Phys. Soc. Jpn.* **54(4)** (1985) 1477-1485.
- [28] Zs. Major, S. B. Dugdale, T. Jarlborg, E. Bruno, B. Ginatempo, J. B. Staunton and J. Poulter. Electronic structure of ordered and disordered Fe₃Pt. *J. Phys.: Condens. Matter*. **15** (2003) 3619–3629.
- [29] D. Paudyal, T. Saha-Dasgupta, and A. Mookerjee. Magnetic properties of X-Pt (X = Fe, Co, Ni) alloy systems. *J. Phys.: Condens. Matter*. **16(13)** (2004) 2317-2334.
- [30] M. Shirai, H. Maeshima, and N. Suzuki. Spin polarized band structure of Cu₃Au-type compounds MPt₃ (M=V, Cr, Mn, Fe, Co). *J. Magn. Magn. Mater.* **140-144** (1995) 105-106.
- [31] J. M. Sanchez, J. L. Morán-Lopez, C. Leroux and M. C. Cadeville. Magnetic properties and chemical ordering in Co-Pt. *J. Phys.: Condens. Matter*. **1** (1989) 1789-1798.

- [32] G. Barcaro, L. Sementa, F. R. Negreiros, R. Ferrando, and A. Fortunelli. Interface Effects on the Magnetism of CoPt-Supported Nanostructures. *Nano Lett.* **11** (2011) 5542–5547.
- [33] C. Petit, S. Rusponi, and H. Brune. Magnetic properties of cobalt and cobalt–platinum nanocrystals investigated by magneto-optical Kerr effect. *J. Appl. Phys.* **95(8)** (2004) 4251-4260.
- [34] S. Karoui, H. Amara, B. Legrand, and F. Ducastelle. Magnetism: the driving force of order in CoPt, a first-principles study. *J. Phys.: Condens. Matter.* **25** (2013) 056005.
- [35] J. M. Montejano-Carrizales, F. Aguilera-Granja, C. Goyhenex, V. Pierron-Bohnes, J. L. Morán-López. Structural, electronic and magnetic properties of $\text{Co}_n\text{Pt}_{M-n}$, for $M=13, 19,$ and 55 , from first principles. *J. Magn. Magn. Mater.* **355** (2014) 215-224.
- [36] W. F. Hu, H. K. Yuan, H. Chen, G. Z. Wang, and G. L. Zhang. Structural and magnetic properties of CoPt clusters. *Phys. Lett. A* **378** (2014) 198–206.
- [37] I. G. Shuttleworth. Strain engineering of H/transition metal systems. *Surf. Sci.* **661** (2017) 49-59
- [38] P. Andreazza, V. Pierron-Bohnes, F. Tournus, C. Andreazza-Vignolle, and V. Dupuis. Structure and order in cobalt/platinum-type nanoalloys: from thin films to supported clusters. *Surf. Sci. Reps.* **70** (2015) 188–258.
- [39] P. Giannozzi, S. Baroni, N. Bonini, M. Calandra, R. Car, C. Cavazzoni, D. Ceresoli, G. L. Chiarotti, M. Cococcioni, I. Dabo, A. Dal Corso, S. Fabris, G. Fratesi, S. de Gironcoli, R. Gebauer, U. Gerstmann, C. Gougoussis, A. Kokalj, M. Lazzeri, L. Martin-Samos, N. Marzari, F. Mauri, R. Mazzarello, S. Paolini, A. Pasquarello, L. Paulatto, C. Sbraccia, S. Scandolo, G. Sclauzero, A.P. Seitsonen, A. Smogunov, P. Umari, and R. M. Wentzcovitch. QUANTUM ESPRESSO: a modular and open-source software project for quantum simulations of materials. *J. Phys.: Condens. Matter.* **21** (2009) 395502.

- [40] The x.pbe-n-rrkjus_psl.1.0.0.UPF, x.pbe-spn-rrkjus_psl.1.0.0.UPF, Pt.pbe-spf-rrkjus_psl.1.0.0.UPF, x.rel-pbe-n-rrkjus_psl.1.0.0.UPF, x.rel-pbe-spn-rrkjus_psl.1.0.0.UPF, and Pt.rel-pbe-spf-rrkjus_psl.1.0.0.UPF, where x=Pt, Fe or Co, pseudopotentials were used from the Quantum ESPRESSO pseudopotential data base: <http://www.quantum-espresso.org/pseudopotentials>.
- [41] A. Dal Corso. Pseudopotentials periodic table: From H to Pu. *Comput. Mater. Sci.* **95** (2014) 337-350.
- [42] M. Methfessel, and A.T. Paxton. High-precision sampling for Brillouin-zone integration in metals. *Phys. Rev. B: Condens. Matter* **40** (1989) 3616–3621.
- [43] W. Setyawan, and S. Curtarolo. High-throughput electronic band structure calculations: Challenges and tools. *Comput. Mater. Sci.* **49(2)** (2010) 299-312.

Table 1. Summary of the structural parameters of the (a) Pt-Fe, and the (b) Pt-Co alloys. C denotes collinear (scalar relativistic) and NC non-collinear (vector relativistic) simulations. ‘Exptl’ denotes the results from experimental investigations. The results in these tables were determined with zero strain ($\varepsilon = 0\%$).

(a)

Structure	Pseudopotential semi-core states	a (Å)			c (Å)		
		C	NC	Exptl	C	NC	Exptl
PtFe	-	3.873	3.872	3.86[12]	3.759	3.733	3.788[12]
	Pt (sp) Fe (sp)	3.858	3.857		3.746	3.703	
	Pt (spf) Fe (sp)	3.848	3.848		3.746	3.694	
Pt ₃ Fe	-	3.920	3.918	3.864[12]			
	Pt (sp) Fe (sp)	3.904	3.903				
	Pt (spf) Fe (sp)	3.889	3.895				
PtFe ₃	-	3.722	3.660	3.75[12]			
	Pt (sp) Fe (sp)	3.727	3.634				
	Pt (spf) Fe (sp)	3.727	3.630				

(b)

Structure	Pseudopotential semi-core states	a (Å)			c (Å)		
		C	NC	Exptl	C	NC	Exptl
PtCo	-	3.825	3.827	3.803[38]	3.720	3.697	3.701[38]
	Pt (sp) Co (sp)	3.801	3.825		3.711	3.683	
	Pt (spf) Co (sp)	3.791	3.824		3.708	3.683	
Pt ₃ Co	-	3.892	3.898	3.854[38]			
	Pt (sp) Co (sp)	3.876	3.894				
	Pt (spf) Co (sp)	3.869	3.893				
PtCo ₃	-	3.671	3.672	3.663[38]			
	Pt (sp) Co (sp)	3.646	3.670				
	Pt (spf) Co (sp)	3.642	3.668				

Table 2. Summary of the j-resolved d occupancies $N_{d,j}^M(\varepsilon = 0\%)$ and its fractional change $\delta N_{d,j}^M(\varepsilon = \pm 5\%)$ under strain for the Pt-Fe and Pt-Co systems.

System	State	$N_{d,j}^M(\varepsilon = 0\%)$ (states)	$\delta N_{d,j}^M(\varepsilon = +5\%)$ (%)	$\delta N_{d,j}^M(\varepsilon = -5\%)$ (%)
Pt₃Fe	Pt d j=1.5	9.251	0.999	-0.999
	Pt d j=2.5	8.580	0.094	-0.094
	Fe d j=1.5	6.580	-0.978	0.978
	Fe d j=2.5	6.464	-1.479	1.479
PtFe	Pt d j=1.5	9.249	0.772	-0.772
	Pt d j=2.5	8.646	0.420	-0.420
	Fe d j=1.5	6.776	-0.970	0.970
	Fe d j=2.5	6.658	-1.542	1.542
PtFe₃	Pt d j=1.5	9.170	1.416	-1.416
	Pt d j=2.5	8.535	1.754	-1.754
	Fe d j=1.5	6.953	-0.844	0.844
	Fe d j=2.5	6.768	-1.166	1.166
Pt₃Co	Pt d j=1.5	9.270	0.991	-0.991
	Pt d j=2.5	8.565	-0.018	0.018
	Co d j=1.5	7.827	-0.432	0.432
	Co d j=2.5	7.707	-1.275	1.275
PtCo	Pt d j=1.5	9.250	0.616	-0.616
	Pt d j=2.5	8.583	-0.017	0.017
	Co d j=1.5	7.828	-1.220	1.220
	Co d j=2.5	7.821	0.143	-0.143
PtCo₃	Pt d j=1.5	9.261	0.591	-0.591
	Pt d j=2.5	8.597	0.350	-0.350
	Co d j=1.5	7.869	-0.959	0.959
	Co d j=2.5	7.690	-1.637	1.637

Table S1. Tabulated charge populations for the (a) Pt₃Fe, (b) PtFe, and (c) PtFe₃ alloys. $q_{0\%}$ is the occupation of the state when the strain $\varepsilon = 0\%$ and δq is the change in occupation of the state when then strain $\varepsilon \neq 0\%$. C and NC denote collinear and non-collinear simulations, respectively.

(a)

Pt₃Fe	Pseudopotential semi-core states	q _{0%} (states)		δq (states)		δq (states)	
		ε = 0%		ε = +5%		ε = -5%	
		C	NC	C	NC	C	NC
Pt	-	10.0628	10.0642	0.0322	0.0294	-0.0531	-0.0504
	Pt (sp) Fe (sp)	17.9218	17.9030	0.0350	0.0333	-0.0464	-0.0451
	Pt (spf) Fe (sp)	31.9192	31.9019	0.0350	0.0331	-0.0473	-0.0455
Pt s	-	0.4119	0.4114	0.0032	0.0057	-0.0034	-0.0060
	Pt (sp) Fe (sp)	3.0388	3.0417	0.0069	0.0098	-0.0205	-0.0225
	Pt (spf) Fe (sp)	3.0380	3.0413	0.0076	0.0101	-0.0219	-0.0231
Pt p	-	0.9209	0.9554	0.0006	-0.0021	-0.0264	-0.0225
	Pt (sp) Fe (sp)	5.9980	5.9979	0.0005	0.0005	-0.0007	-0.0008
	Pt (spf) Fe (sp)	5.9980	5.9978	0.0005	0.0006	-0.0008	-0.0008
Pt d	-	8.7301	8.6975	0.0284	0.0257	-0.0233	-0.0220
	Pt (sp) Fe (sp)	8.8850	8.8635	0.0276	0.0228	-0.0251	-0.0219
	Pt (spf) Fe (sp)	8.8834	8.8629	0.0269	0.0224	-0.0246	-0.0216
Fe	-	7.7596	7.7513	-0.0840	-0.0736	0.1348	0.1242
	Pt (sp) Fe (sp)	15.4061	15.4231	-0.0806	-0.0790	0.1442	0.1441
	Pt (spf) Fe (sp)	15.4149	15.4278	-0.0842	-0.0803	0.1502	0.1470
Fe s	-	0.2968	0.2939	0.0072	0.0096	-0.0044	-0.0071
	Pt (sp) Fe (sp)	2.9117	2.9152	0.0137	0.0156	-0.0203	-0.0222
	Pt (spf) Fe (sp)	2.9104	2.9144	0.0143	0.0158	-0.0209	-0.0223
Fe p	-	1.0103	0.9962	-0.0059	0.0015	-0.0142	-0.0213
	Pt (sp) Fe (sp)	5.9992	5.9992	0.0002	0.0002	-0.0003	-0.0003
	Pt (spf) Fe (sp)	5.9992	5.9992	0.0001	0.0001	-0.0003	-0.0003
Fe d	-	6.4524	6.4613	-0.0853	-0.0847	0.1535	0.1525
	Pt (sp) Fe (sp)	6.4951	6.5087	-0.0944	-0.0948	0.1649	0.1667
	Pt (spf) Fe (sp)	6.5054	6.5142	-0.0988	-0.0963	0.1713	0.1697

(b)

PtFe	Pseudopotential semi-core states	q _{0%} (states)		δq (states)		δq (states)	
		ε = 0%		ε = +5%		ε = -5%	
		C	NC	C	NC	C	NC
Pt	-	10.0819	10.0884	0.0778	0.0721	-0.0997	-0.0956
	Pt (sp) Fe (sp)	17.9849	17.9586	0.0617	0.0617	-0.0750	-0.0773
	Pt (spf) Fe (sp)	31.9829	31.9554	0.0616	0.0618	-0.0758	-0.0786
Pt s	-	0.4343	0.4337	0.0060	0.0075	-0.0062	-0.0074
	Pt (sp) Fe (sp)	3.0700	3.0689	0.0224	0.0249	-0.0299	-0.0312
	Pt (spf) Fe (sp)	3.0695	3.0676	0.0225	0.0252	-0.0301	-0.0312
Pt p	-	0.9119	0.9508	0.0301	0.0253	-0.0473	-0.0404
	Pt (sp) Fe (sp)	5.9972	5.9970	0.0008	0.0008	-0.0011	-0.0012
	Pt (spf) Fe (sp)	5.9972	5.9969	0.0008	0.0009	-0.0011	-0.0011
Pt d	-	8.7357	8.7038	0.0417	0.0394	-0.0462	-0.0477
	Pt (sp) Fe (sp)	8.9176	8.8927	0.0386	0.0360	-0.0438	-0.0450
	Pt (spf) Fe (sp)	8.9165	8.8910	0.0382	0.0358	-0.0447	-0.0461
Fe	-	7.8891	7.8812	-0.0715	-0.0654	0.0896	0.0845
	Pt (sp) Fe (sp)	15.5805	15.5953	-0.0689	-0.0702	0.0912	0.0951
	Pt (spf) Fe (sp)	15.5834	15.5997	-0.0692	-0.0711	0.0924	0.0967
Fe s	-	0.3083	0.3045	0.0070	0.0081	-0.0037	-0.0055
	Pt (sp) Fe (sp)	2.9359	2.9358	0.0289	0.0294	-0.0354	-0.0360
	Pt (spf) Fe (sp)	2.9340	2.9339	0.0298	0.0301	-0.0348	-0.0356
Fe p	-	1.0054	0.9934	0.0087	0.0139	-0.0196	-0.0254
	Pt (sp) Fe (sp)	5.9990	5.9989	0.0002	0.0003	-0.0005	-0.0004
	Pt (spf) Fe (sp)	5.9989	5.9989	0.0003	0.0003	-0.0004	-0.0004
Fe d	-	6.5754	6.5833	-0.0872	-0.0874	0.1129	0.1154
	Pt (sp) Fe (sp)	6.6457	6.6606	-0.0981	-0.0999	0.1270	0.1315
	Pt (spf) Fe (sp)	6.6504	6.6669	-0.0992	-0.1015	0.1277	0.1327

(c)

PtFe ₃	Pseudopotential semi-core states	q _{0%} (states)		δq (states)		δq (states)	
		ε = 0%		ε = +5%		ε = -5%	
		C	NC	C	NC	C	NC
Pt	-	10.0121	10.0093	0.1021	0.1307	-0.1924	-0.2667
	Pt (sp) Fe (sp)	18.0252	17.9388	0.0732	0.1018	-0.1608	-0.2151
	Pt (spf) Fe (sp)	32.0251	31.9347	0.0738	0.1044	-0.1618	-0.2219
Pt s	-	0.4597	0.4576	0.0078	0.0080	-0.0109	-0.0123
	Pt (sp) Fe (sp)	3.1039	3.0884	0.0268	0.0332	-0.0374	-0.0452
	Pt (spf) Fe (sp)	3.1041	3.0877	0.0268	0.0335	-0.0375	-0.0458
Pt p	-	0.8718	0.9096	0.0431	0.0512	-0.0582	-0.0577
	Pt (sp) Fe (sp)	5.9962	5.9953	0.0012	0.0014	-0.0014	-0.0012
	Pt (spf) Fe (sp)	5.9962	5.9953	0.0012	0.0014	-0.0014	-0.0012
Pt d	-	8.6806	8.6421	0.0512	0.0715	-0.1233	-0.1967
	Pt (sp) Fe (sp)	8.9251	8.8550	0.0452	0.0673	-0.1220	-0.1685
	Pt (spf) Fe (sp)	8.9251	8.8520	0.0458	0.0694	-0.1229	-0.1748
Fe	-	7.9743	7.9727	-0.0302	-0.0389	0.0605	0.0865
	Pt (sp) Fe (sp)	15.6919	15.7273	-0.0439	-0.0536	0.0757	0.1010
	Pt (spf) Fe (sp)	15.6921	15.7292	-0.0442	-0.0545	0.0762	0.1041
Fe s	-	0.3187	0.3166	0.0020	0.0071	-0.0047	-0.0085
	Pt (sp) Fe (sp)	2.9445	2.9235	0.0457	0.0415	-0.0433	-0.0447
	Pt (spf) Fe (sp)	2.9445	2.9225	0.0459	0.0415	-0.0434	-0.0450
Fe p	-	0.9742	0.9617	0.0126	0.0361	-0.0376	-0.0602
	Pt (sp) Fe (sp)	5.9985	5.9983	0.0005	0.0005	-0.0005	-0.0005
	Pt (spf) Fe (sp)	5.9985	5.9983	0.0005	0.0005	-0.0005	-0.0005
Fe d	-	6.6814	6.6944	-0.0447	-0.0821	0.1028	0.1552
	Pt (sp) Fe (sp)	6.7489	6.8055	-0.0900	-0.0955	0.1195	0.1462
	Pt (spf) Fe (sp)	6.7490	6.8085	-0.0904	-0.0966	0.1202	0.1496

Table S2. Tabulated charge populations for the (a) Pt₃Co, (b) PtCo, and (c) PtCo₃ alloys. $q_{0\%}$ is the occupation of the state when the strain $\varepsilon = 0\%$ and δq is the change in occupation of the state when then strain $\varepsilon \neq 0\%$. C and NC denote collinear and non-collinear simulations, respectively.

(a)

Pt ₃ Co	Pseudopotential semi-core states	q _{0%} (states)		δq (states)		δq (states)	
		ε = 0%		ε = +5%		ε = -5%	
		C	NC	C	NC	C	NC
Pt	-	10.0179	10.0188	0.0379	0.0356	-0.0521	-0.0489
	Pt (sp) Co (sp)	17.8785	17.8632	0.0391	-0.0526	-0.0425	-0.0408
	Pt (spf) Co (sp)	31.8773	31.8634	0.0391	0.0368	-0.0422	-0.0404
Pt s	-	0.4094	0.4087	0.0056	0.0083	-0.0050	-0.0075
	Pt (sp) Co (sp)	3.0310	3.0354	0.0081	-0.0034	-0.0191	-0.0203
	Pt (spf) Co (sp)	3.0306	3.0356	0.0084	0.0105	-0.0194	-0.0203
Pt p	-	0.9140	0.9484	0.0011	-0.0012	-0.0235	-0.0193
	Pt (sp) Co (sp)	5.9979	5.9979	0.0006	0.0004	-0.0007	-0.0008
	Pt (spf) Co (sp)	5.9979	5.9979	0.0006	0.0005	-0.0007	-0.0008
Pt d	-	8.6945	8.6617	0.0313	0.0285	-0.0237	-0.0221
	Pt (sp) Co (sp)	8.8496	8.8300	0.0305	-0.0497	-0.0227	-0.0198
	Pt (spf) Co (sp)	8.8490	8.8302	0.0300	0.0256	-0.0221	-0.0194
Co	-	8.8879	8.8811	-0.0964	-0.0882	0.1278	0.1155
	Pt (sp) Co (sp)	16.5590	16.5681	-0.0813	0.0921	0.1170	0.1134
	Pt (spf) Co (sp)	16.5635	16.5686	-0.0829	-0.0761	0.1181	0.1131
Co s	-	0.2962	0.2938	0.0037	0.0061	-0.0012	-0.0039
	Pt (sp) Co (sp)	2.8769	2.8824	0.0029	-0.0051	-0.0086	-0.0110
	Pt (spf) Co (sp)	2.8767	2.8825	0.0030	0.0060	-0.0090	-0.0111
Co p	-	1.0298	1.0168	-0.0318	-0.0247	0.0211	0.0137
	Pt (sp) Co (sp)	5.9993	5.9994	0.0002	0.0001	-0.0002	-0.0003
	Pt (spf) Co (sp)	5.9993	5.9993	0.0002	0.0002	-0.0002	-0.0002
Co d	-	7.5620	7.5705	-0.0683	-0.0696	0.1077	0.1057
	Pt (sp) Co (sp)	7.6828	7.6864	-0.0844	0.0970	0.1258	0.1246
	Pt (spf) Co (sp)	7.6875	7.6868	-0.0861	-0.0823	0.1272	0.1244

(b)

PtCo	Pseudopotential semi-core states	q _{0%} (states)		δq (states)		δq (states)	
		ε = 0%		ε = +5%		ε = -5%	
		C	NC	C	NC	C	NC
Pt	-	10.0197	10.0233	0.0779	0.0723	-0.0930	-0.0886
	Pt (sp) Co (sp)	17.9410	17.9171	0.0514	0.0529	-0.0650	-0.0647
	Pt (spf) Co (sp)	31.9375	31.9171	0.0531	0.0479	0.0825	-0.0644
Pt s	-	0.4263	0.4255	0.0099	0.0116	-0.0097	-0.0108
	Pt (sp) Co (sp)	3.0632	3.0641	0.0166	0.0198	-0.0281	-0.0272
	Pt (spf) Co (sp)	3.0614	3.0643	0.0183	0.0210	0.0514	-0.0272
Pt p	-	0.9071	0.9457	0.0271	0.0223	-0.0438	-0.0360
	Pt (sp) Co (sp)	5.9972	5.9971	0.0008	0.0008	-0.0010	-0.0011
	Pt (spf) Co (sp)	5.9972	5.9971	0.0008	0.0008	-0.0012	-0.0011
Pt d	-	8.6864	8.6520	0.0408	0.0386	-0.0397	-0.0416
	Pt (sp) Co (sp)	8.8806	8.8559	0.0341	0.0323	-0.0358	-0.0364
	Pt (spf) Co (sp)	8.8791	8.8559	0.0341	0.0261	0.0324	-0.0362
Co	-	8.9452	8.9403	-0.0693	-0.0630	0.0806	0.0750
	Pt (sp) Co (sp)	16.6356	16.6481	-0.0464	-0.0495	0.0730	0.0728
	Pt (spf) Co (sp)	16.6417	16.6489	-0.0511	-0.0945	-1.5200	0.0725
Co s	-	0.3156	0.3120	0.0051	0.0064	-0.0051	-0.0075
	Pt (sp) Co (sp)	2.9185	2.9216	0.0172	0.0174	-0.0270	-0.0278
	Pt (spf) Co (sp)	2.9162	2.9215	0.0189	0.0224	-0.0312	-0.0276
Co p	-	1.0474	1.0381	-0.0196	-0.0146	0.0064	-0.0008
	Pt (sp) Co (sp)	5.9991	5.9992	0.0003	0.0002	-0.0003	-0.0004
	Pt (spf) Co (sp)	5.9991	5.9992	0.0003	0.0001	-0.0028	-0.0004
Co d	-	7.5822	7.5902	-0.0548	-0.0549	0.0793	0.0834
	Pt (sp) Co (sp)	7.7180	7.7274	-0.0638	-0.0672	0.1003	0.1008
	Pt (spf) Co (sp)	7.7264	7.7283	-0.0703	-0.1172	-1.4860	0.1003

(c)

PtCo ₃	Pseudopotential semi-core states	q _{0%} (states)		δq (states)		δq (states)	
		ε = 0%		ε = +5%		ε = -5%	
		C	NC	C	NC	C	NC
Pt	-	9.9834	10.0009	0.1146	0.1049	-0.1275	-0.1174
	Pt (sp) Co (sp)	17.9928	17.9720	0.0628	0.0652	-0.0927	-0.0842
	Pt (spf) Co (sp)	31.9933	31.9557	0.0600	0.0813	-0.0964	-0.0687
Pt s	-	0.4381	0.4396	0.0137	0.0144	-0.0114	-0.0119
	Pt (sp) Co (sp)	3.0852	3.0970	0.0266	0.0215	-0.0235	-0.0293
	Pt (spf) Co (sp)	3.0931	3.0921	0.0122	0.0266	-0.0320	-0.0243
Pt p	-	0.8758	0.9223	0.0521	0.0434	-0.0509	-0.0406
	Pt (sp) Co (sp)	5.9962	5.9961	0.0011	0.0012	-0.0014	-0.0013
	Pt (spf) Co (sp)	5.9962	5.9961	0.0010	0.0012	-0.0015	-0.0013
Pt d	-	8.6694	8.6389	0.0490	0.0471	-0.0651	-0.0648
	Pt (sp) Co (sp)	8.9115	8.8788	0.0351	0.0426	-0.0680	-0.0534
	Pt (spf) Co (sp)	8.9042	8.8677	0.0469	0.0535	-0.0629	-0.0430
Co	-	8.9790	8.9731	-0.0336	-0.0301	0.0359	0.0318
	Pt (sp) Co (sp)	16.7116	16.7024	-0.0281	-0.0177	0.0440	0.0519
	Pt (spf) Co (sp)	16.7121	16.7064	-0.0273	-0.0215	0.0453	0.0484
Co s	-	0.3263	0.3235	0.0093	0.0102	-0.0084	-0.0096
	Pt (sp) Co (sp)	2.9387	2.9401	0.0280	0.0304	-0.0313	-0.0291
	Pt (spf) Co (sp)	2.9381	2.9417	0.0252	0.0290	-0.0316	-0.0307
Co p	-	1.0463	1.0399	-0.0017	0.0009	-0.0156	-0.0192
	Pt (sp) Co (sp)	5.9988	5.9988	0.0004	0.0004	-0.0004	-0.0004
	Pt (spf) Co (sp)	5.9988	5.9989	0.0003	0.0003	-0.0004	-0.0005
Co d	-	7.6064	7.6097	-0.0412	-0.0412	0.0598	0.0606
	Pt (sp) Co (sp)	7.7741	7.7635	-0.0564	-0.0485	0.0758	0.0813
	Pt (spf) Co (sp)	7.7752	7.7659	-0.0528	-0.0509	0.0773	0.0795

Fig. 1. Models of the (a) MPt_3 ($L1_2$) and (b-c) MPt ($L1_0$) unit cells, where M denotes either Fe or Co. In (a) the M atom is at (0,0,0) and the Pt atoms are at (0.5,0.5,0), (0,0.5,0.5) and (0.5,0,0.5). In (b-c) the M atoms are at (0,0,0) and (0.5,0.5,0), and the Pt atoms are at (0,0.5,0.5) and (0.5,0,0.5). The M_3Pt unit cell is obtained by replacing each Pt (M) atom with M (Pt) in the MPt_3 unit cell.

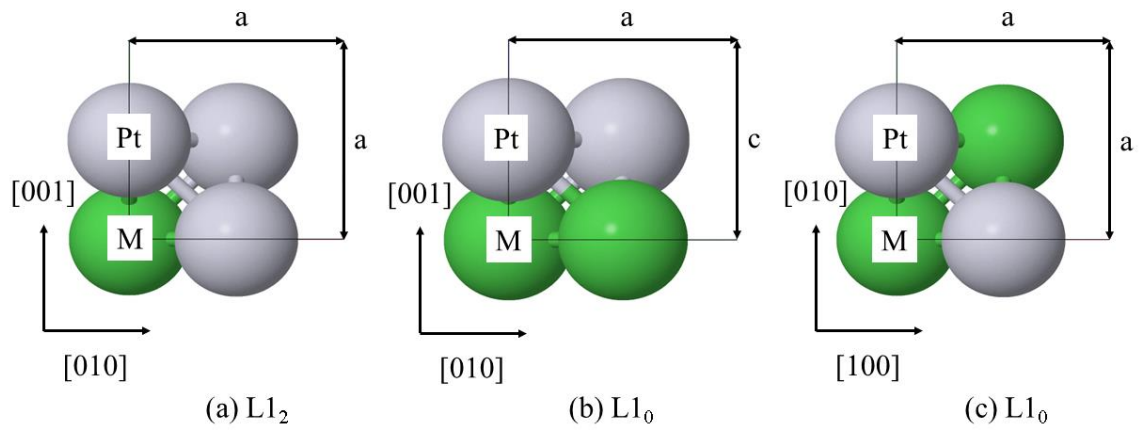


Fig. 2. Magnetic moment μ of the (a) Fe d, and (b) Pt d states for the Pt₃Fe, PtFe and PtFe₃ alloys versus strain ε . The black (grey) lines are from non-collinear (collinear) simulations.

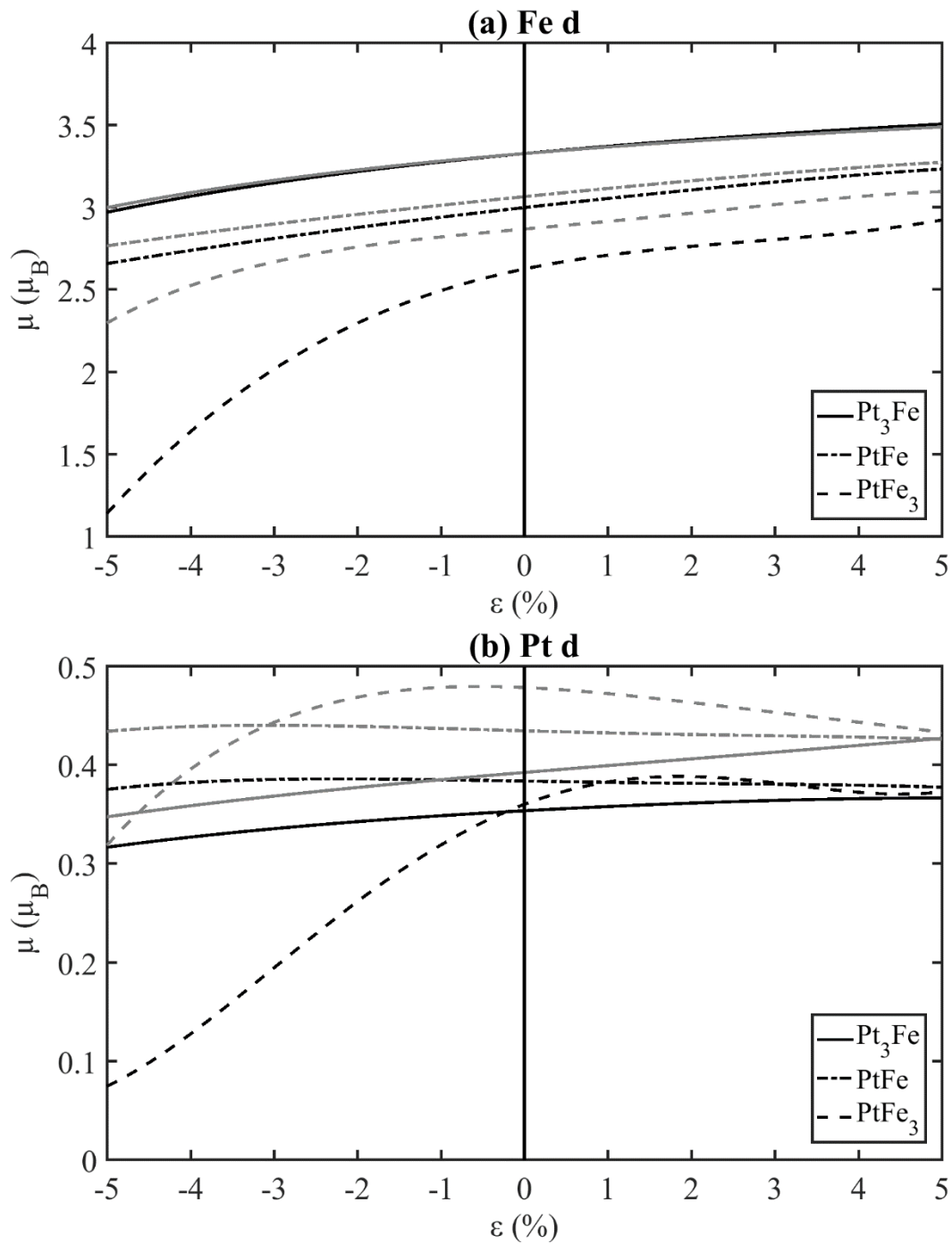


Fig. 3. The variance v of the occupancy $N_{d,j,m_j}^M(\varepsilon)$ for the (a) Pt₃Fe, (b) PtFe and (c) PtFe₃ alloys versus strain ε .

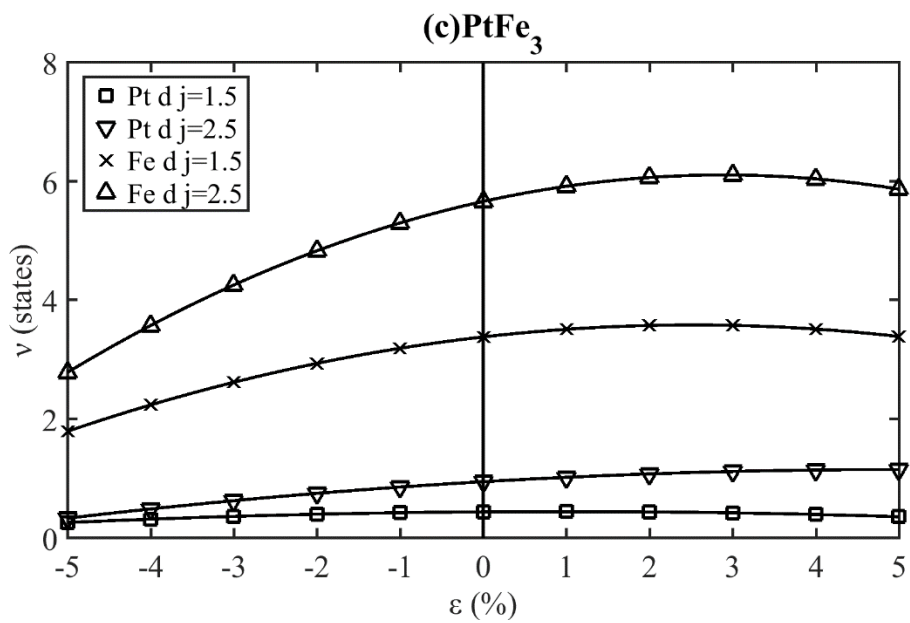
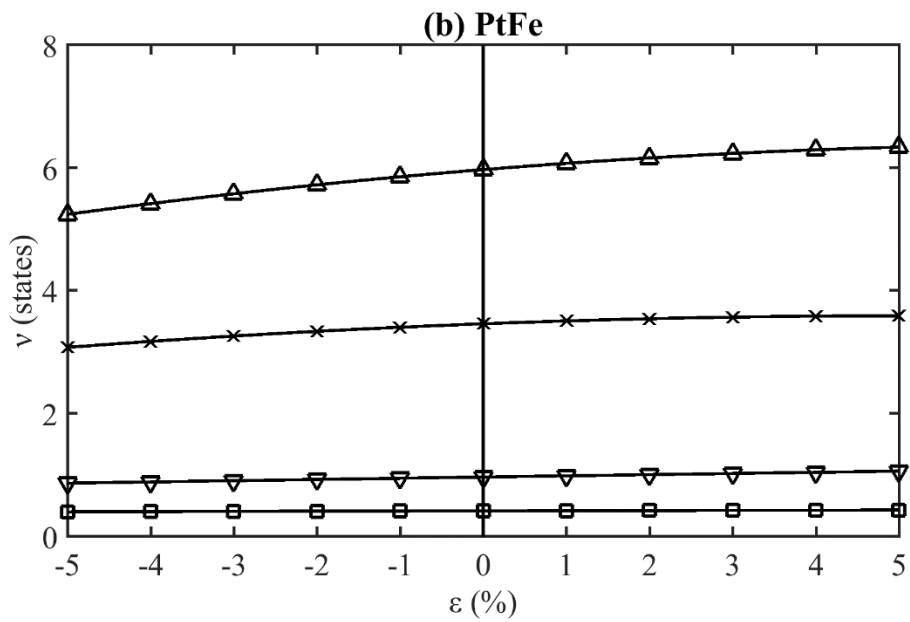
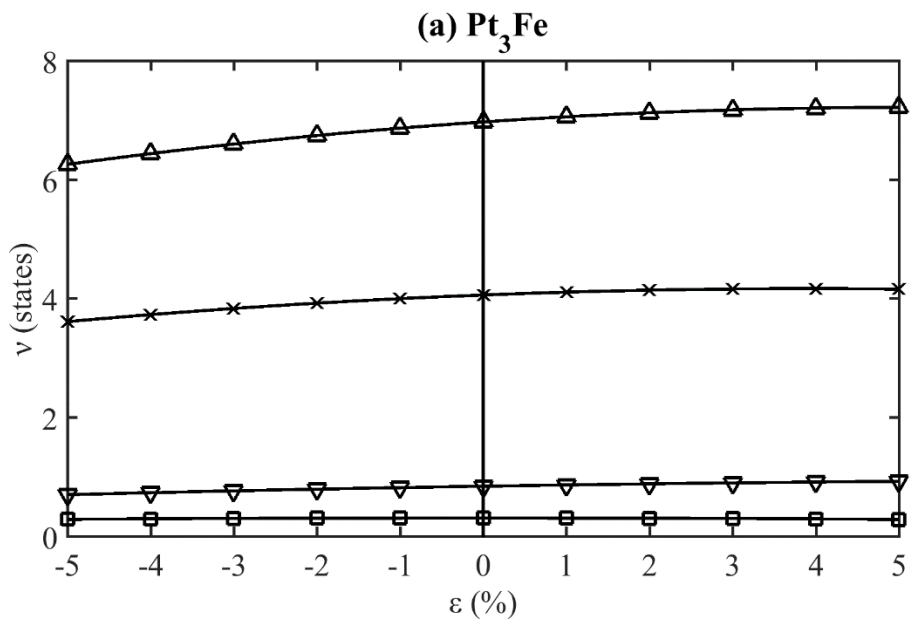
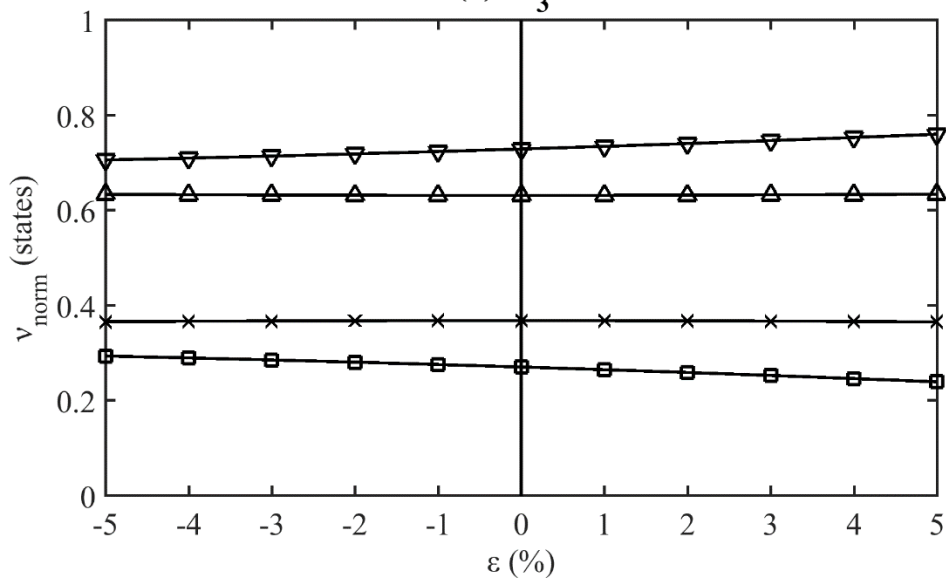
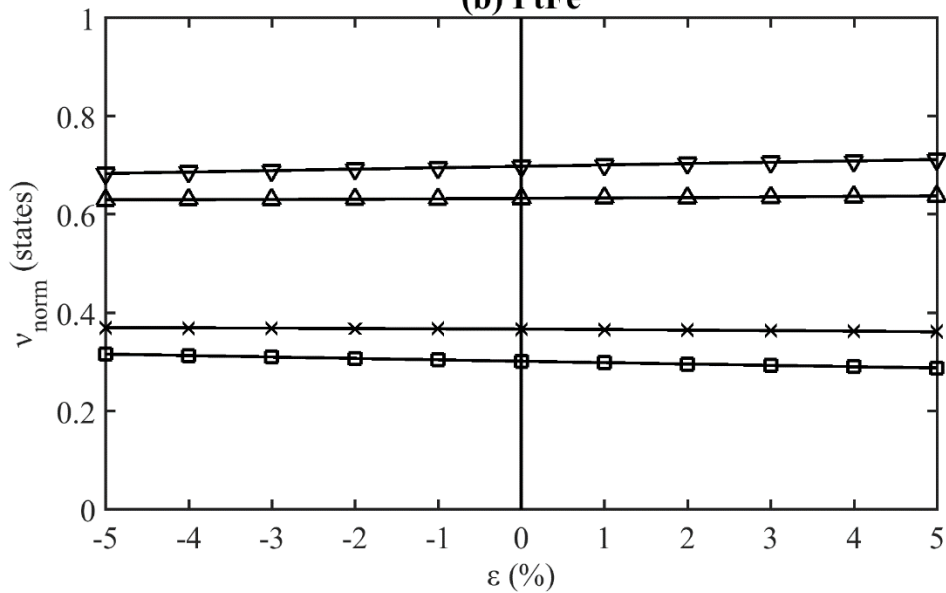


Fig. 4. The normalised variance v_{norm} of the occupancy $N_{d,j,m_j}^M(\varepsilon)$ for the (a) Pt₃Fe, (b) PtFe and (c) PtFe₃ alloys versus strain ε .

(a) Pt₃Fe



(b) PtFe



(c) PtFe₃

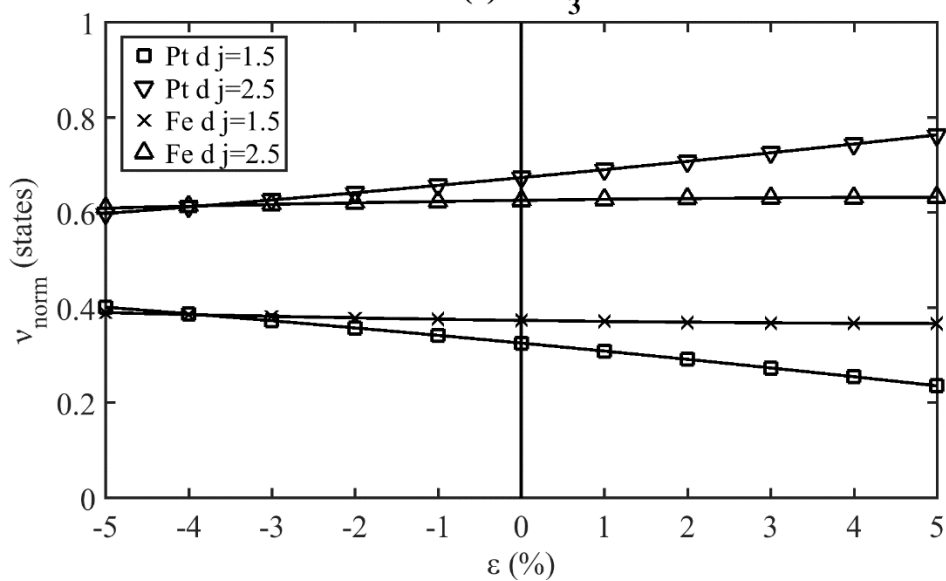
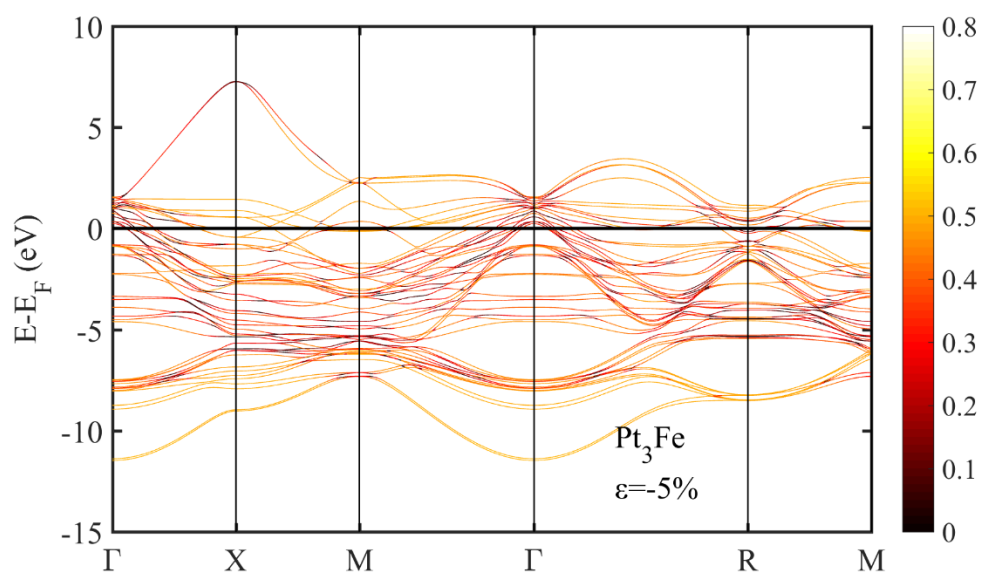
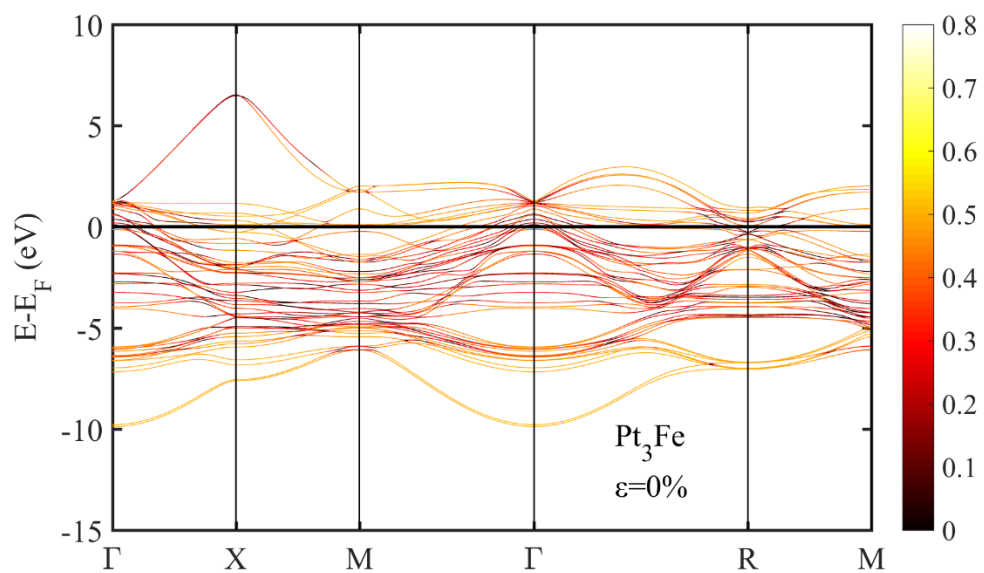
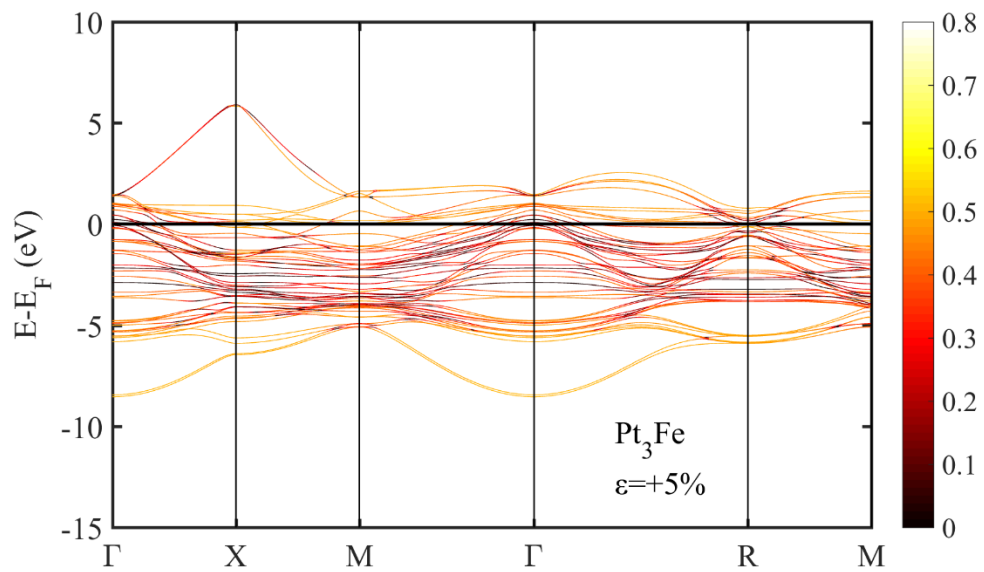
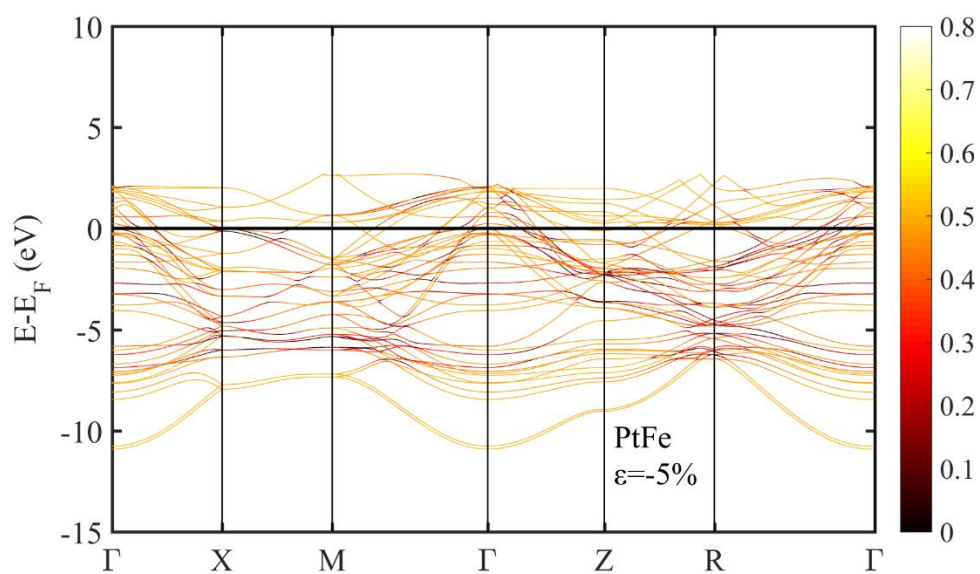
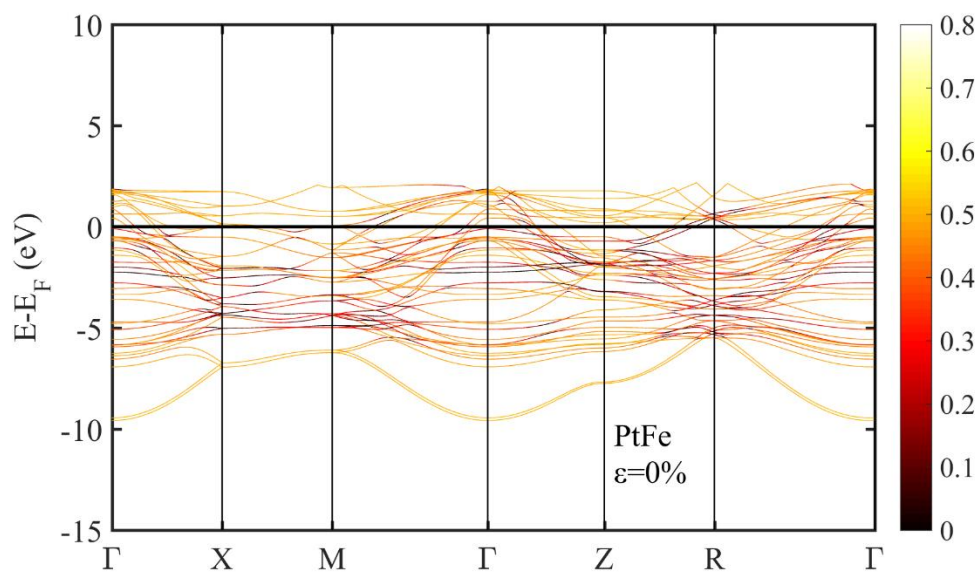
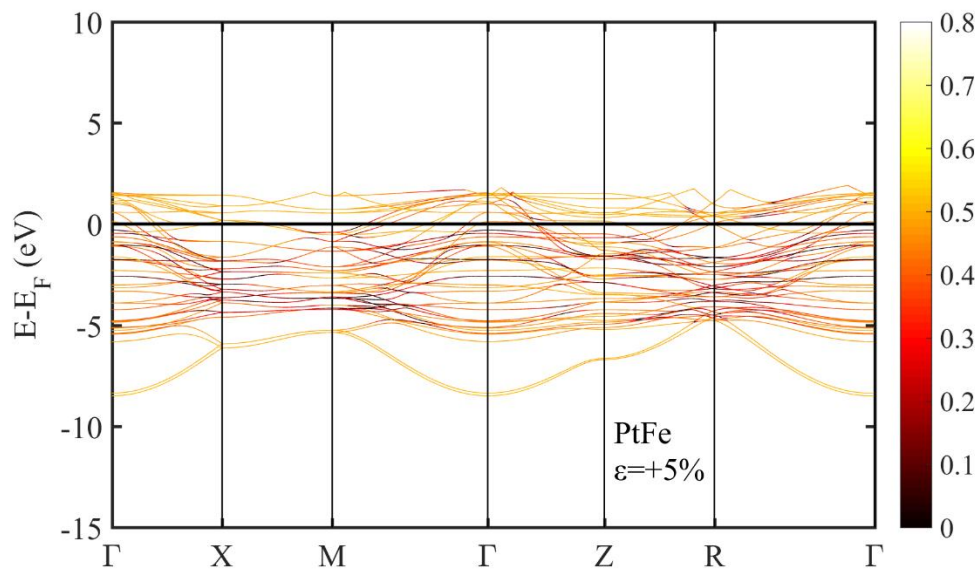


Fig. 5. Band structures of the (a) Pt₃Fe, (b) PtFe, and (c) PtFe₃ alloys for strain $\epsilon=0\%$ and $\pm 5\%$. The colouring is the total spin polarisation $S(k,E)$.

(a)



(b)



(c)

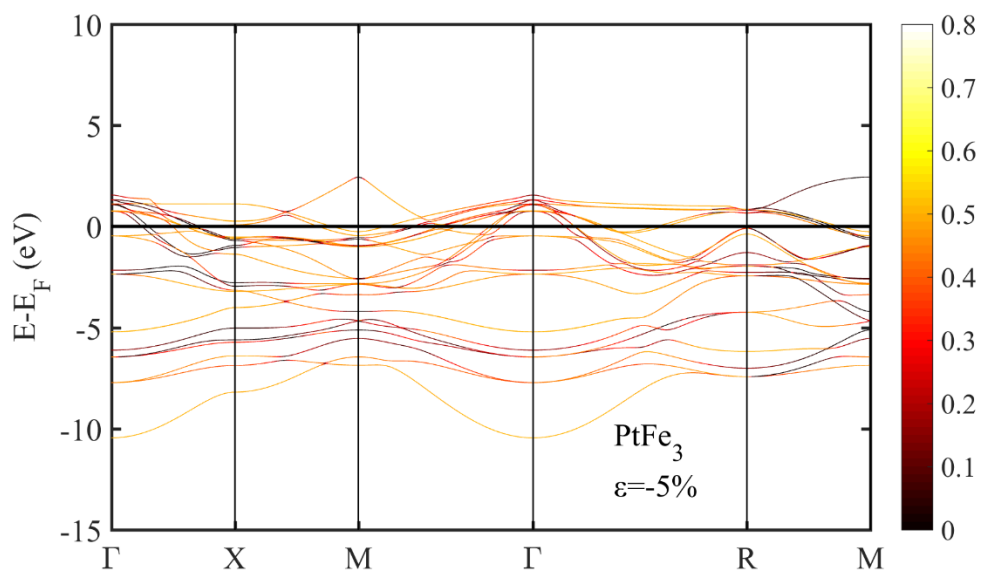
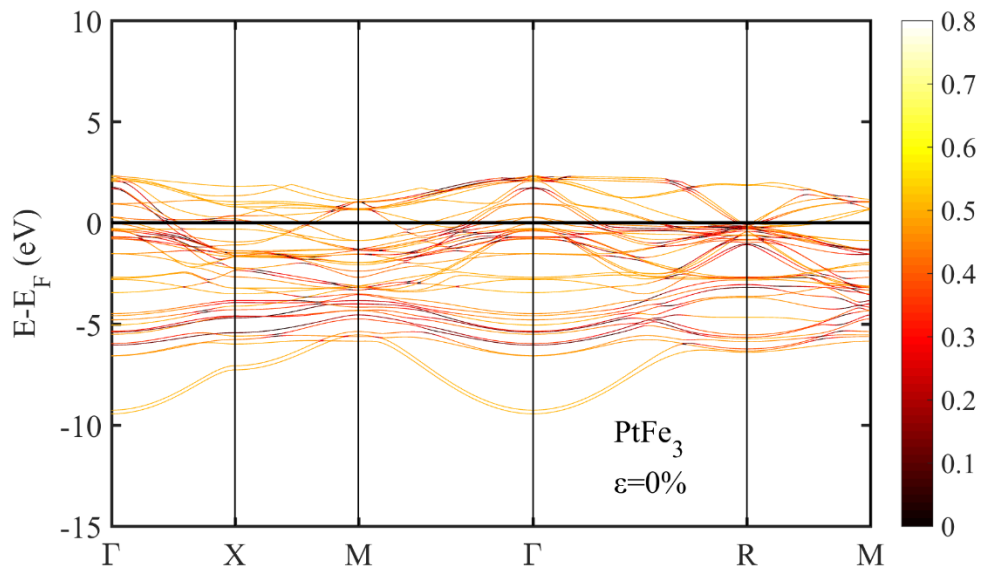
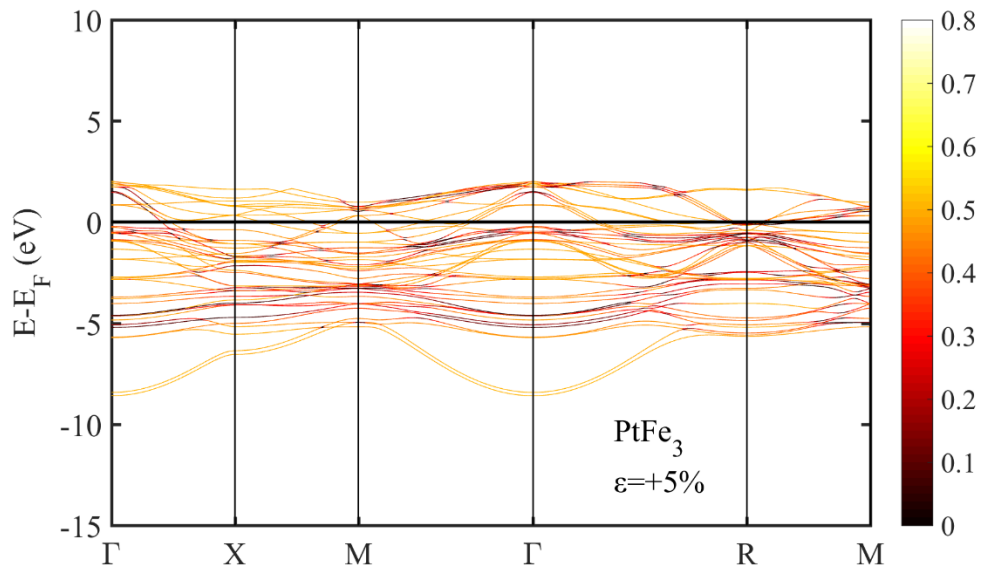


Fig. 6. Magnetic moment μ of the (a) Co d, and (b) Pt d states for the Pt_3Co , PtCo and PtCo_3 alloys versus strain ε . The black (grey) lines are from non-collinear (collinear) simulations.

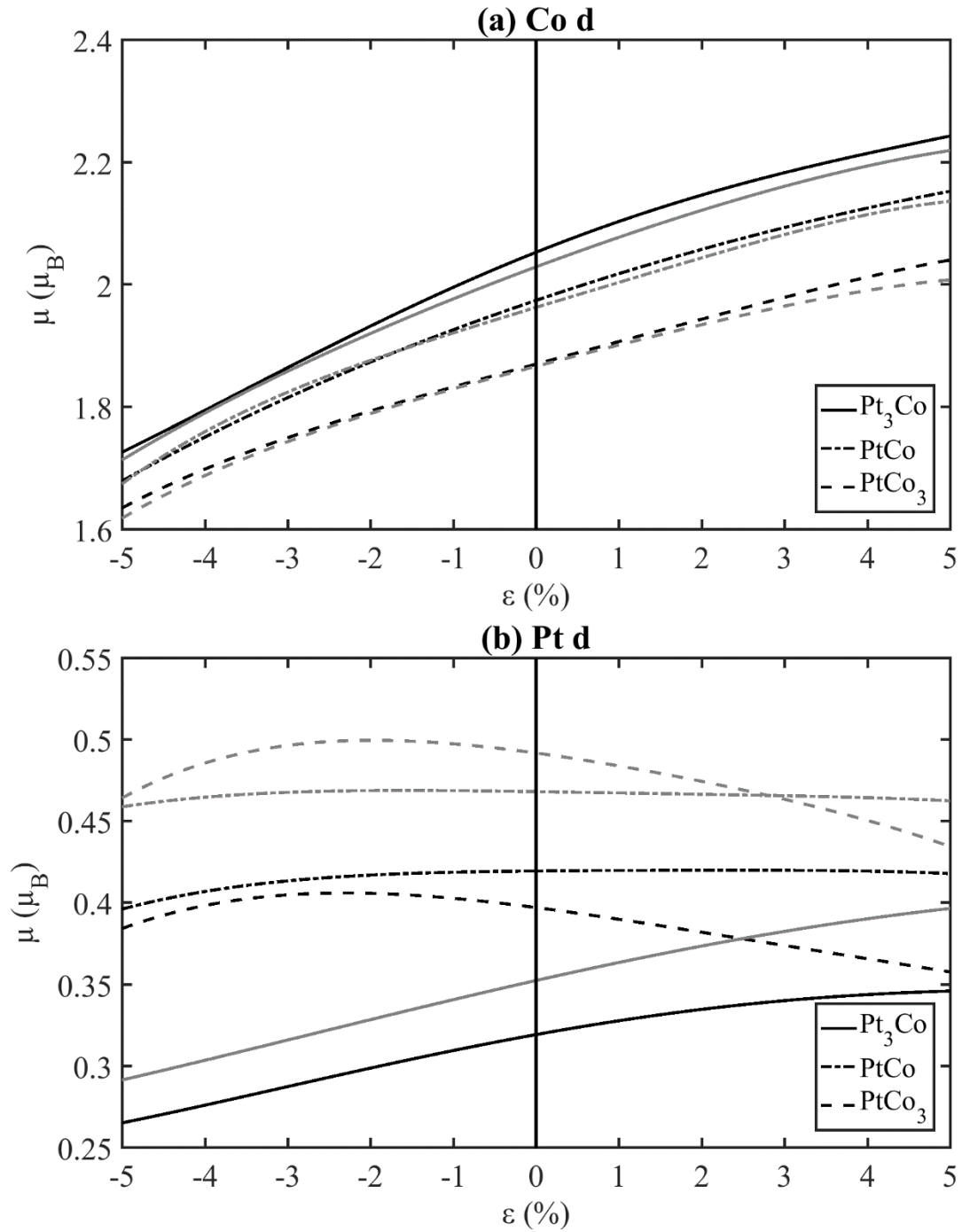
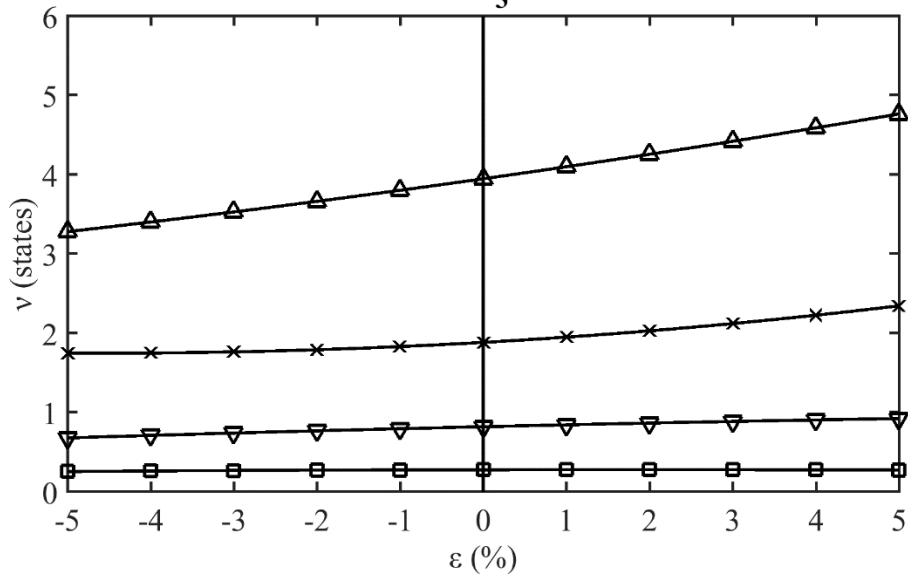
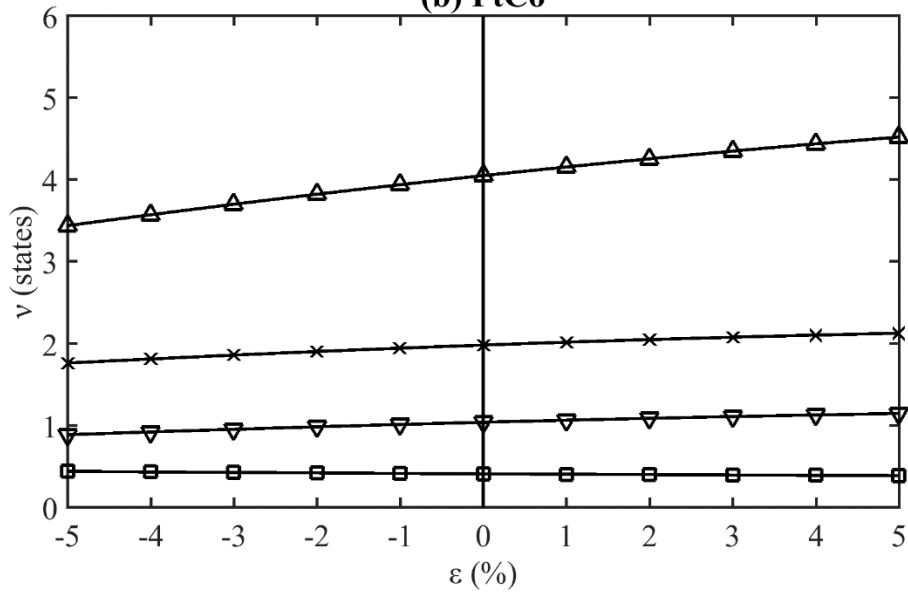


Fig. 7. The variance v of the occupancy $N_{d,j,m_j}^M(\epsilon)$ for the (a) Pt₃Co, (b) PtCo and (c) PtCo₃ alloys versus strain ϵ .

(a) Pt_3Co



(b) PtCo



(c) PtCo_3

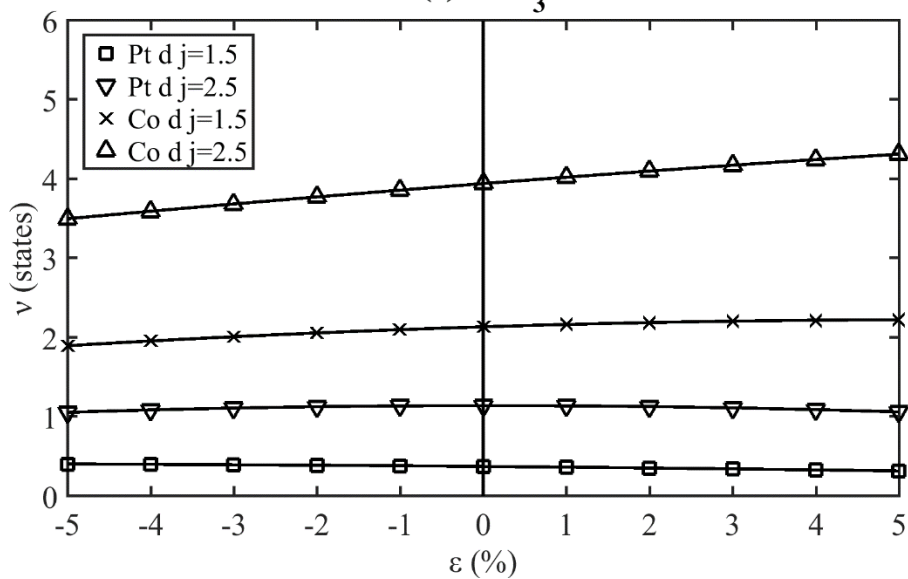
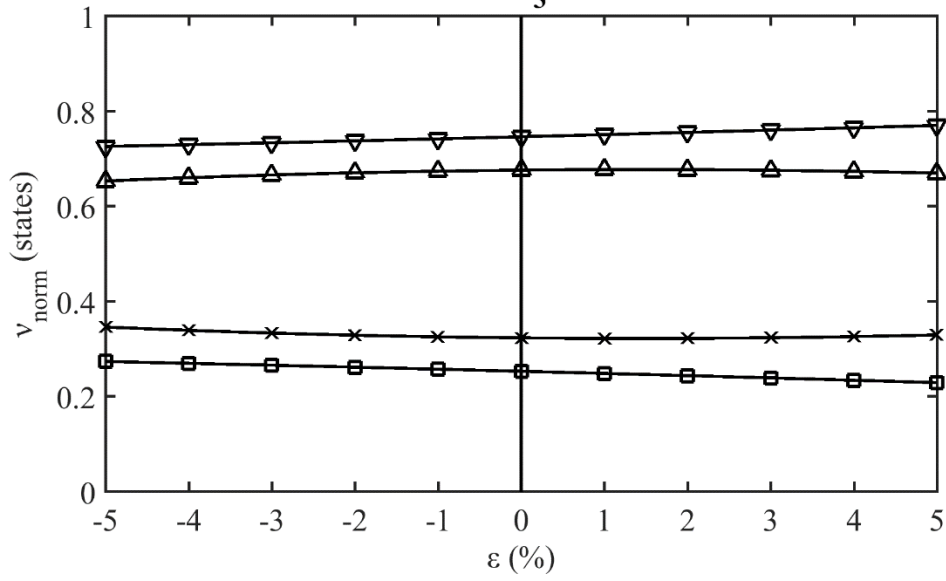
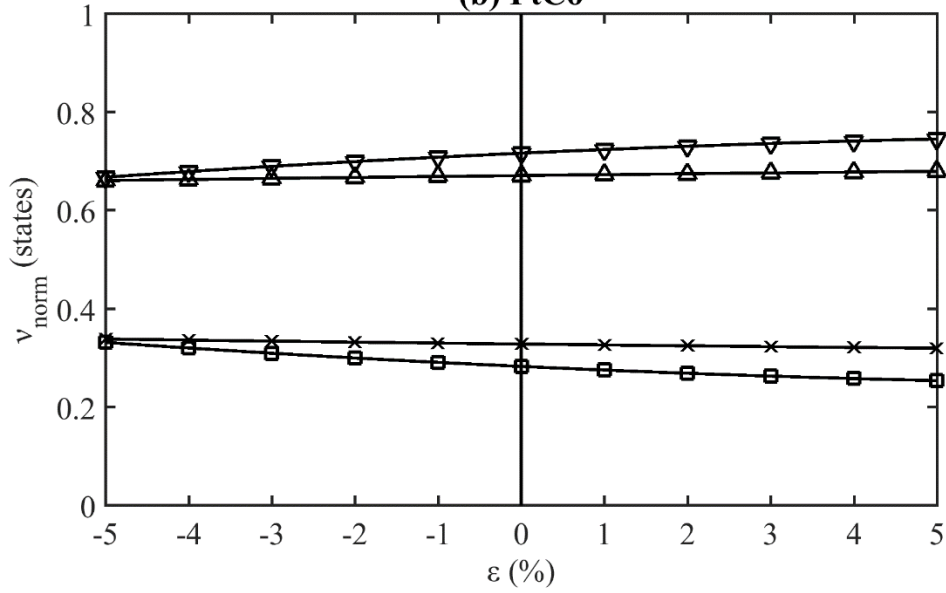


Fig. 8. The normalised variance v_{norm} of the occupancy $N_{d,j,m_j}^M(\epsilon)$ for the (a) Pt₃Co, (b) PtCo and (c) PtCo₃ alloys versus strain ϵ .

(a) Pt₃Co



(b) PtCo



(c) PtCo₃

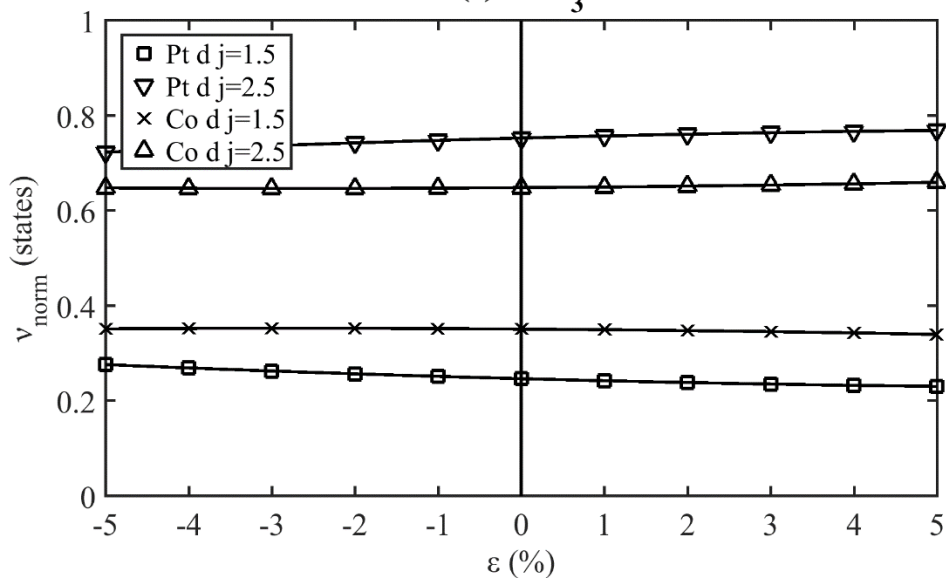
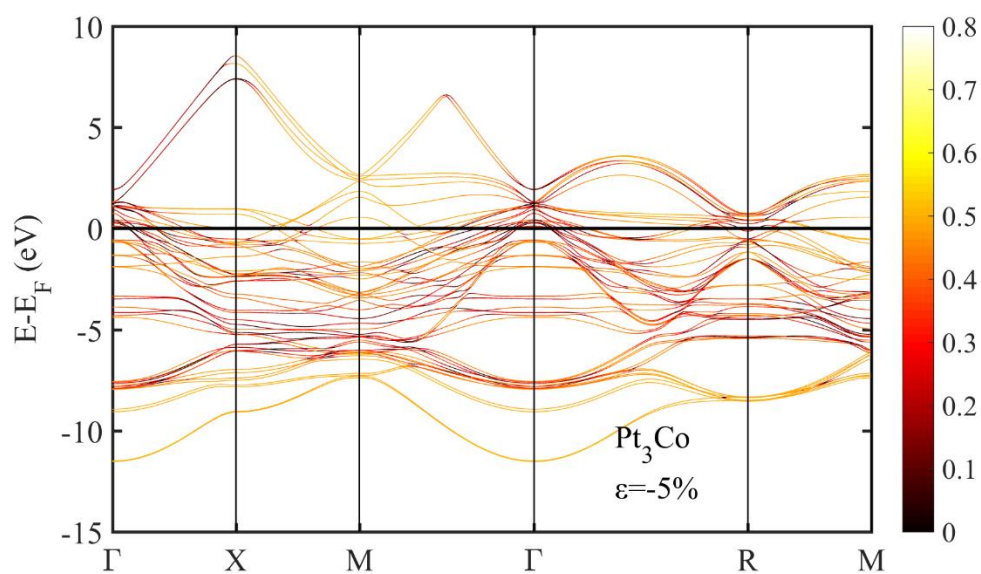
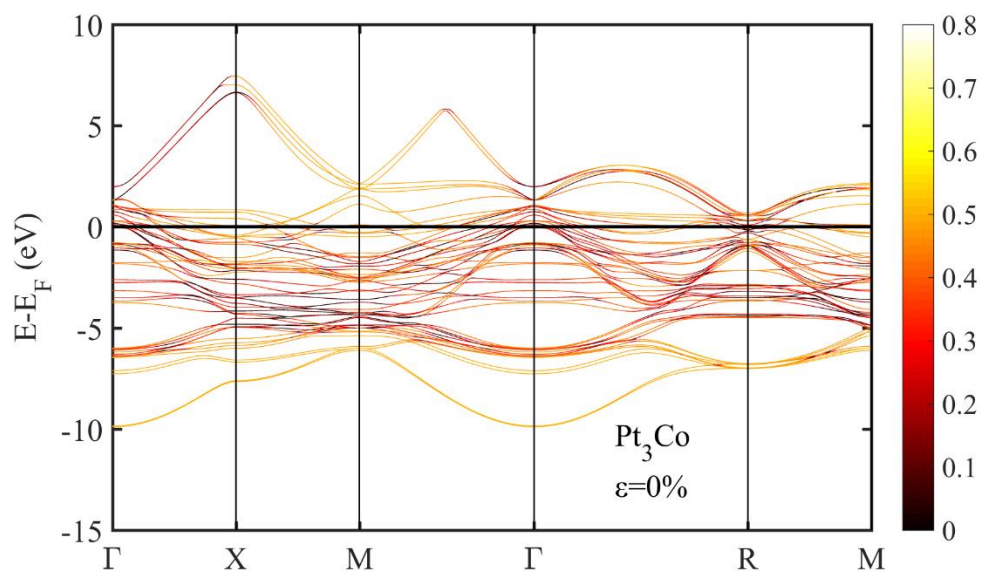
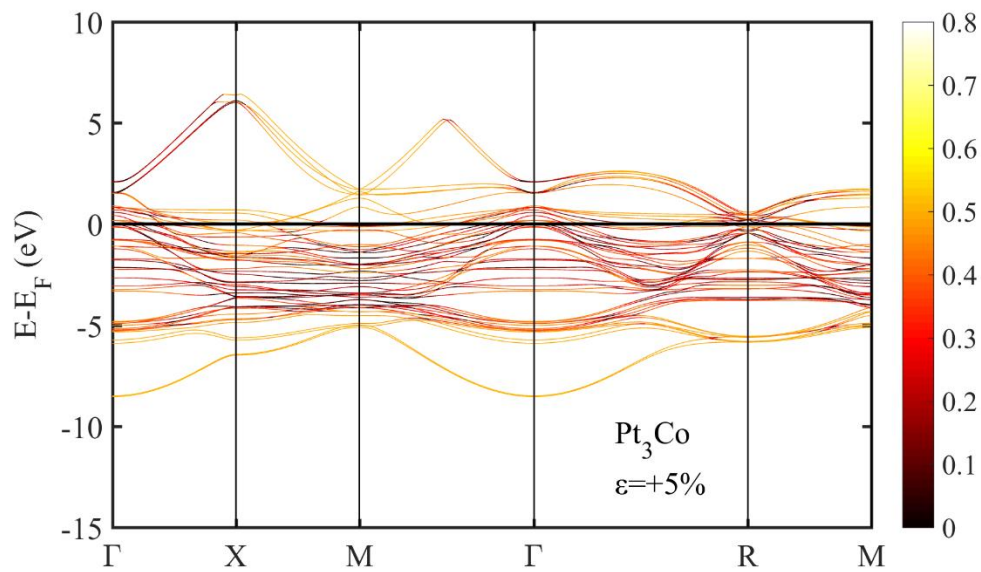
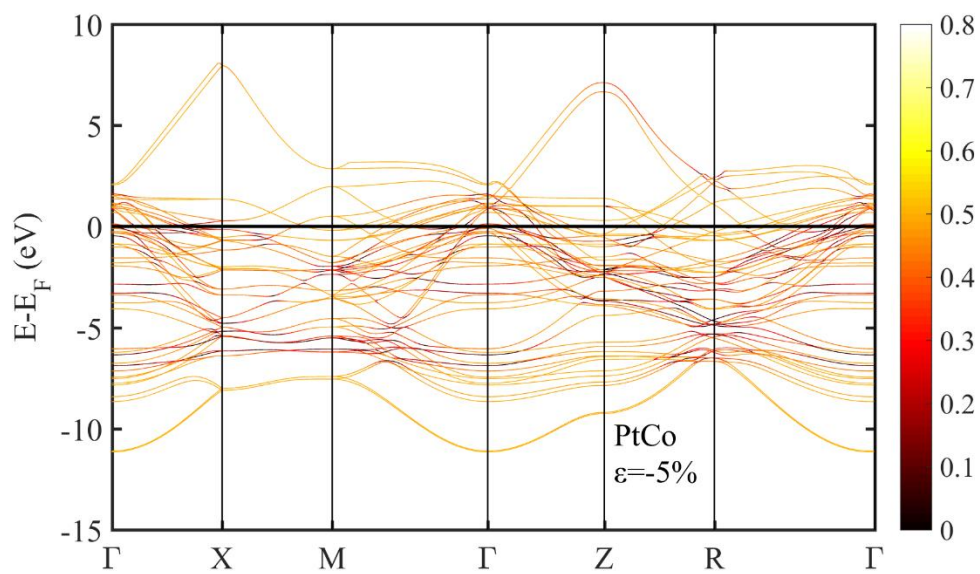
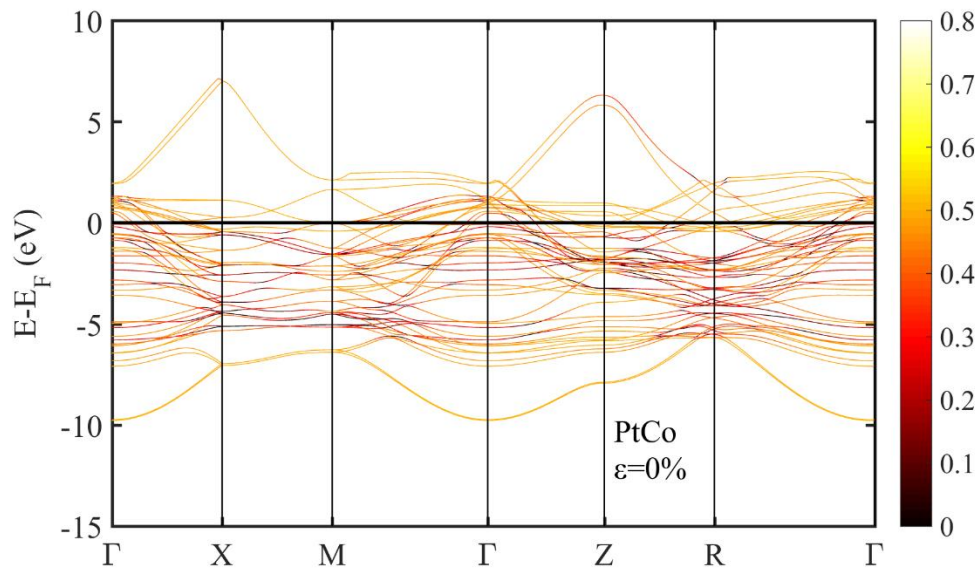
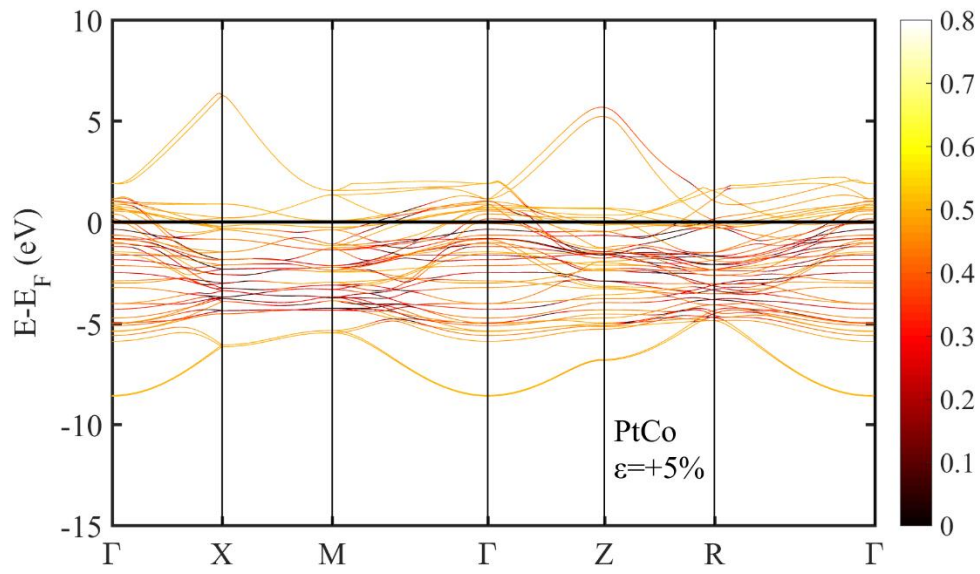


Fig. 9. Band structures of the (a) Pt₃Co, (b) PtCo, and (c) PtCo₃ alloys for strain $\epsilon=0\%$ and $\pm 5\%$. The colouring is the total spin polarisation $S(k,E)$.

(a)



(b)



(c)

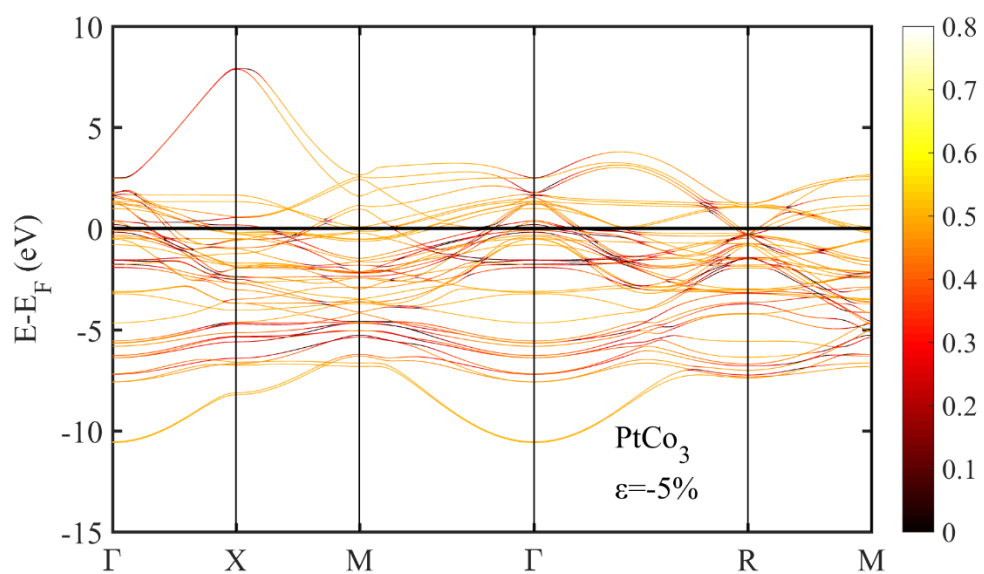
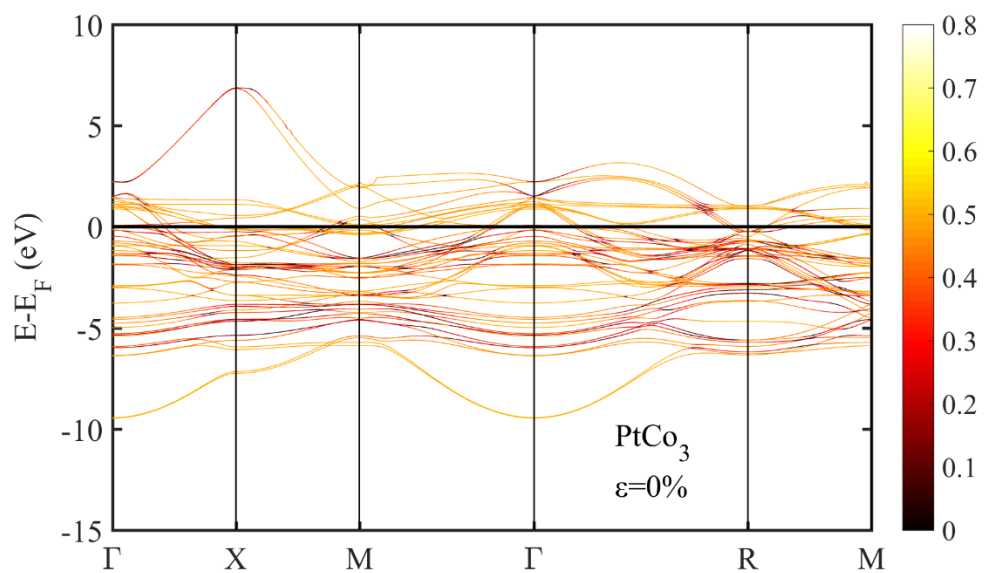
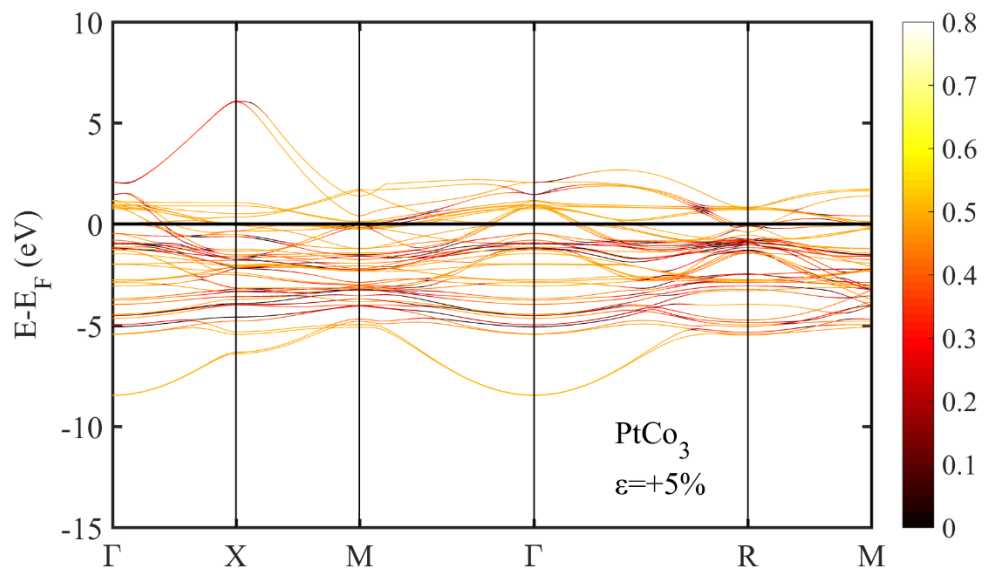
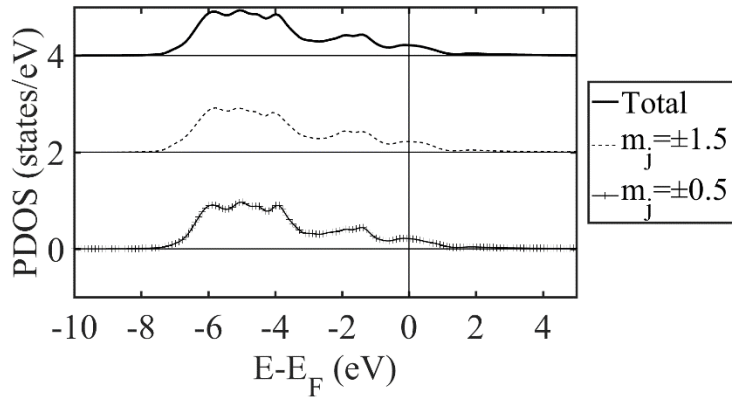


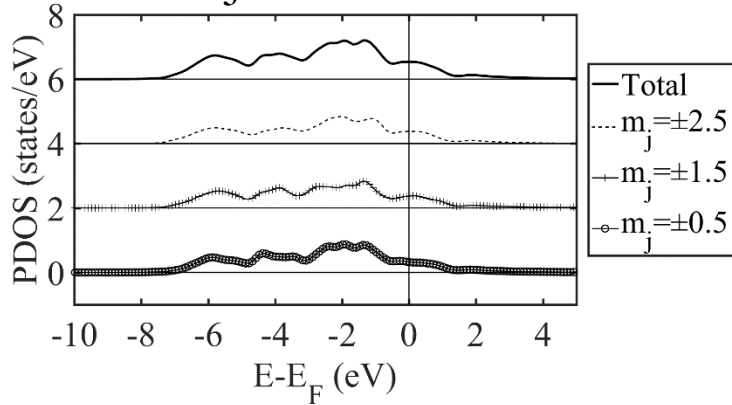
Fig. S1. Total projected density of states (PDOS) curves and the j-resolved curves $\sum_{m_j} n_{d,j,m_j}^M(\varepsilon = 0\%, E)$ for unstrained (a) (i) Pt₃Fe, (ii) PtFe, and (iii) PtFe₃, and (b) (i) Pt₃Co, (ii) PtCo, and (iii) PtCo₃ systems. The total projected density of states curves are labelled ‘Total’ and are the average of the j-resolved curves. The j-resolved curves are labelled according to their m_j components. Subsequent curves are offset vertically for clarity.

(a) (i)

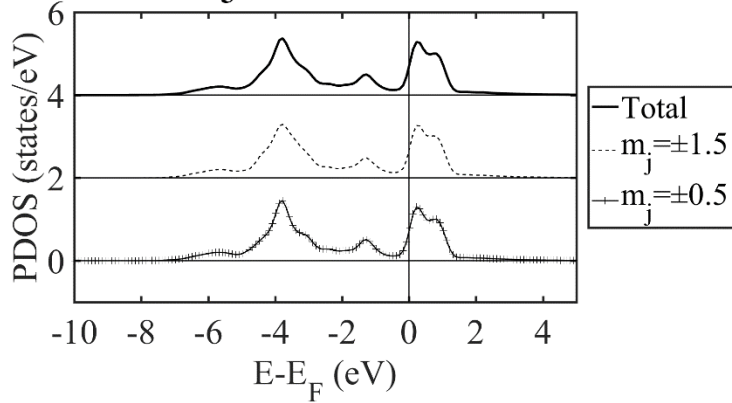
Pt₃Fe: Pt d j=1.5



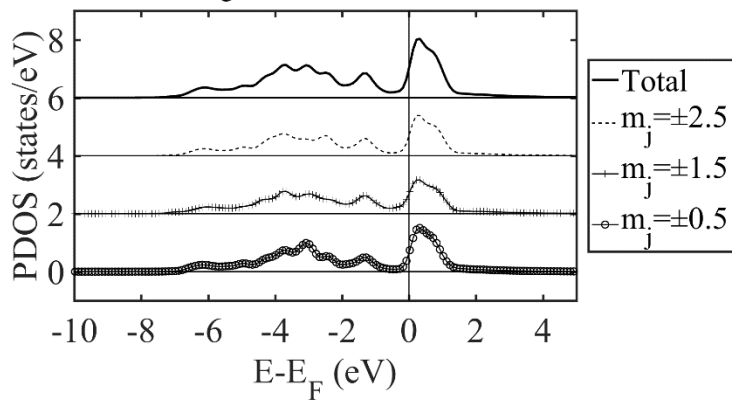
Pt₃Fe: Pt d j=2.5



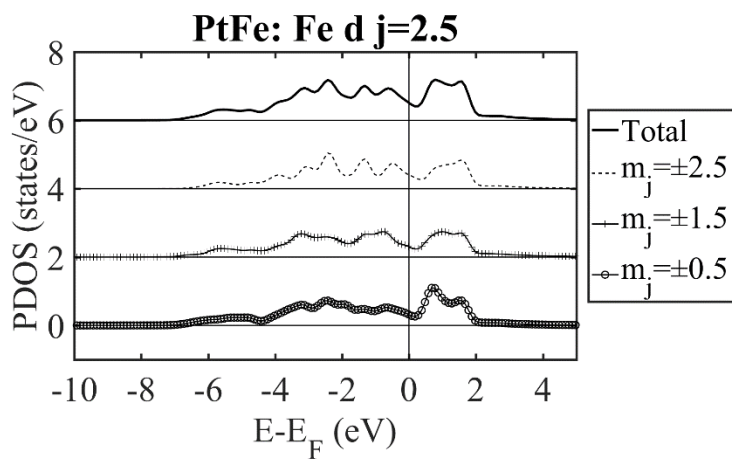
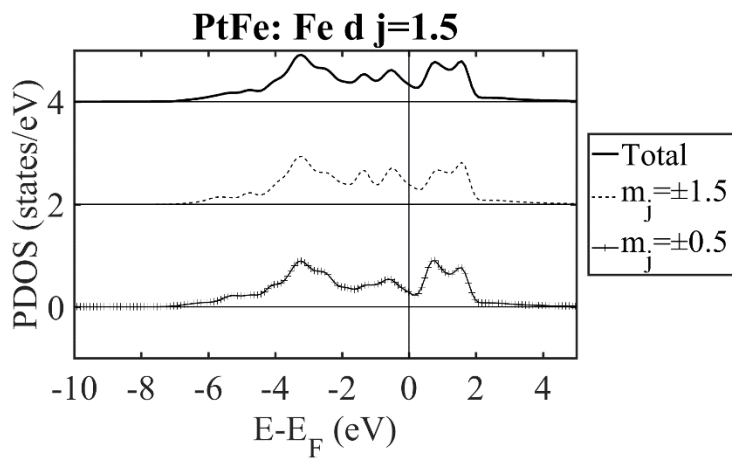
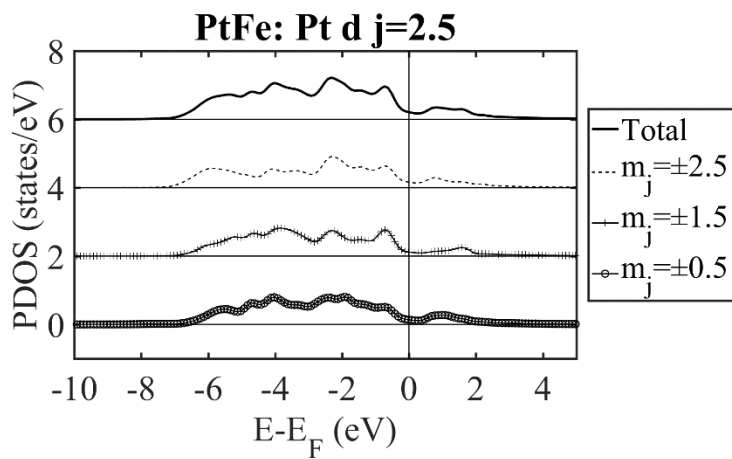
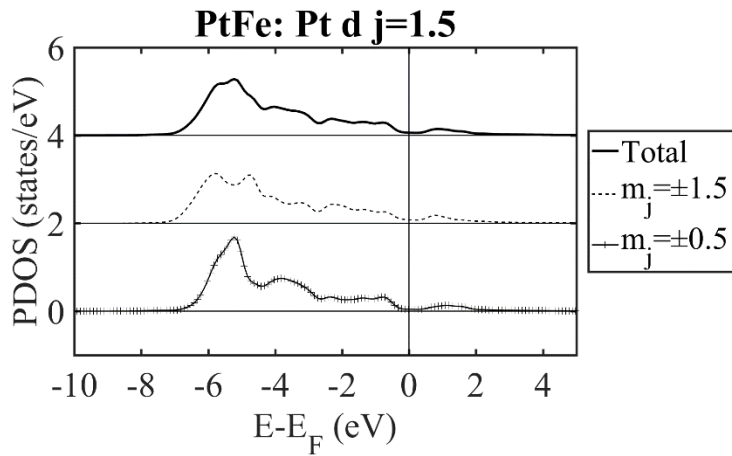
Pt₃Fe: Fe d j=1.5



Pt₃Fe: Fe d j=2.5

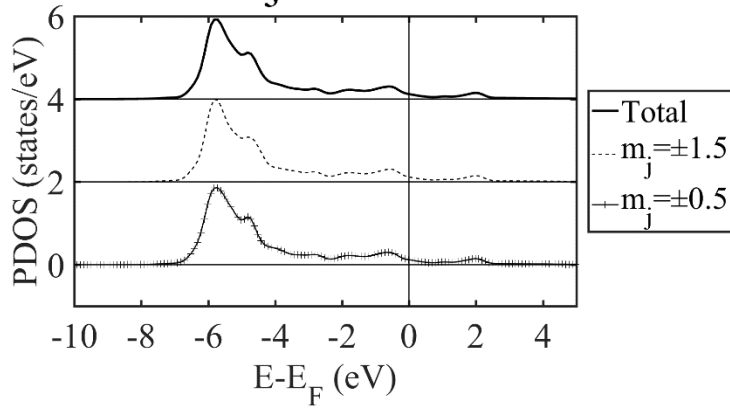


(a) (ii)

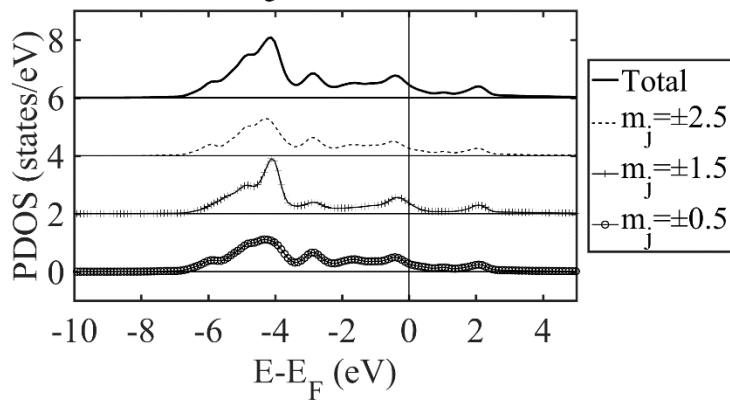


(a) (iii)

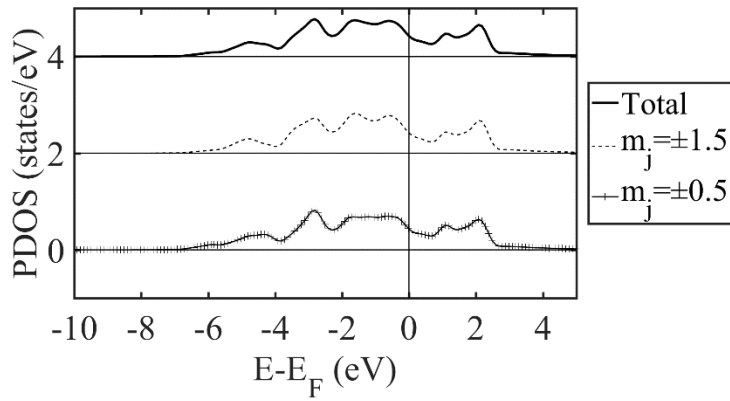
PtFe₃: Pt d j=1.5



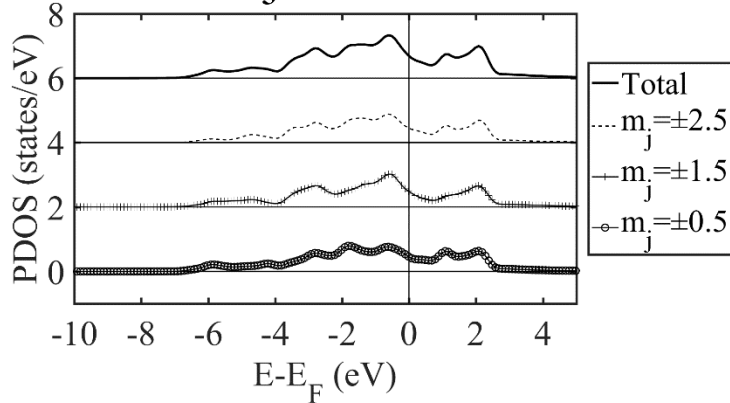
PtFe₃: Pt d j=2.5



PtFe₃: Fe d j=1.5

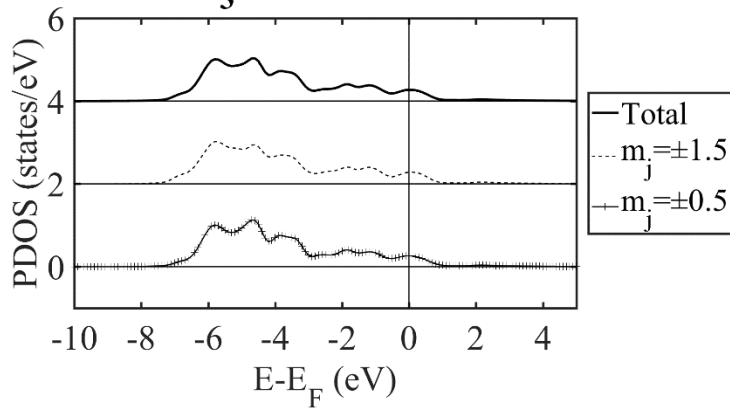


PtFe₃: Fe d j=2.5

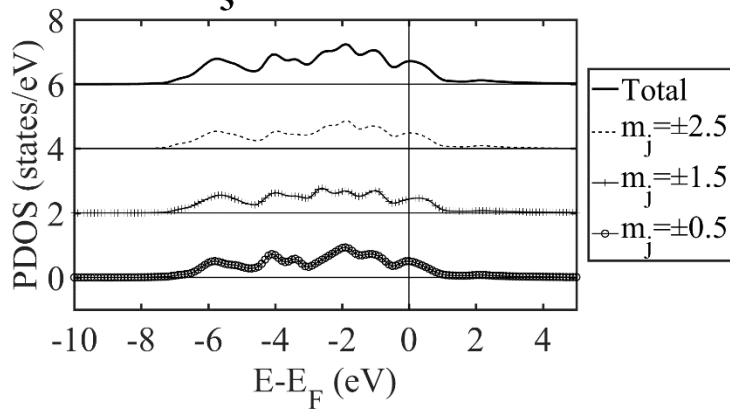


(b) (i)

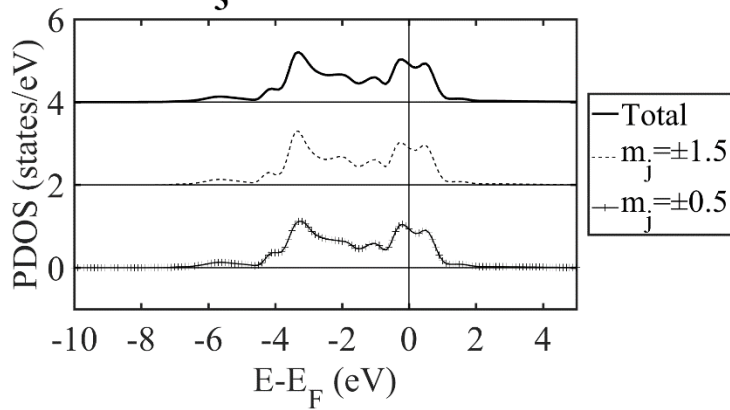
Pt₃Co: Pt d j=1.5



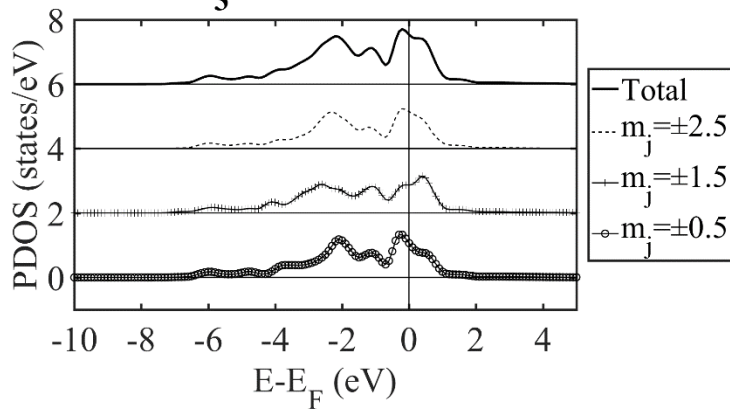
Pt₃Co: Pt d j=2.5



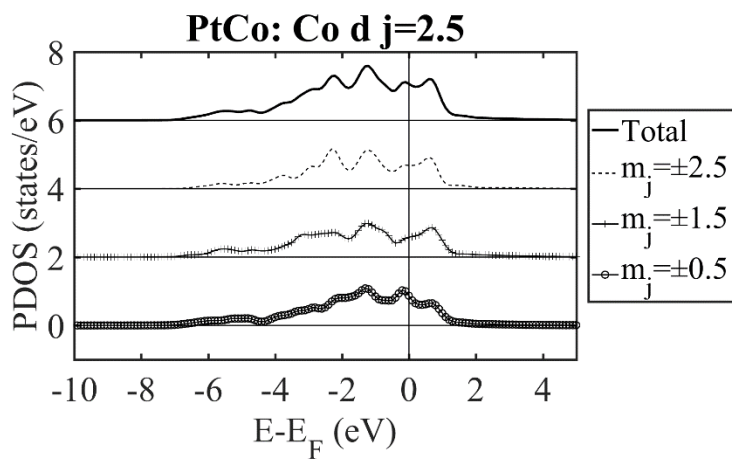
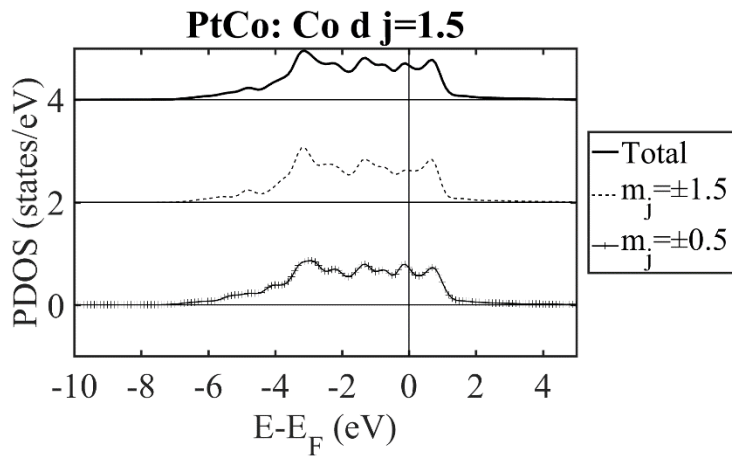
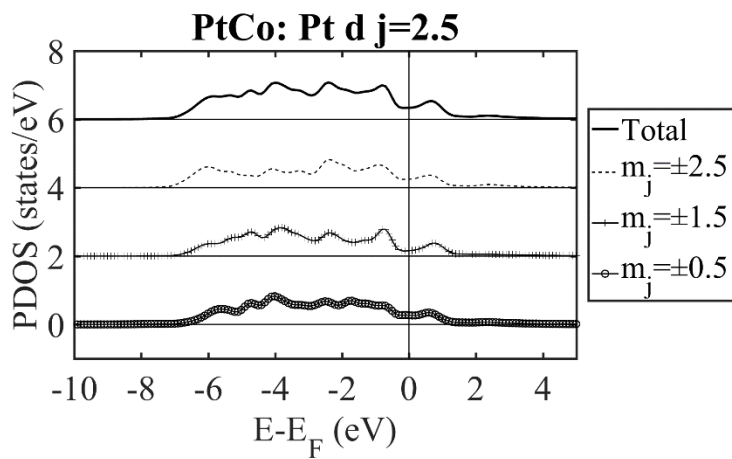
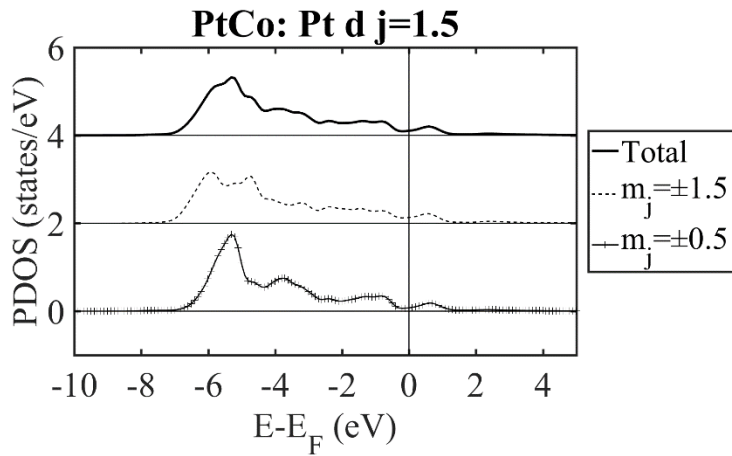
Pt₃Co: Co d j=1.5



Pt₃Co: Co d j=2.5

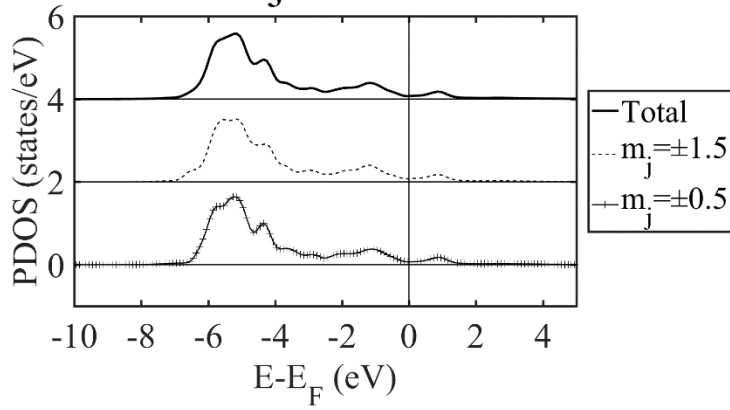


(b) (ii)

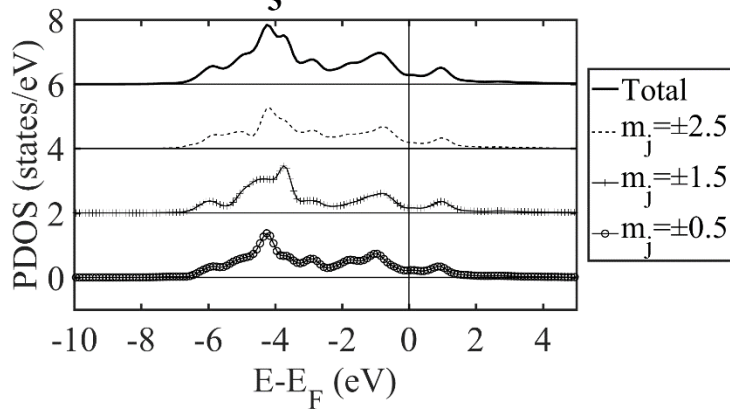


(b) (iii)

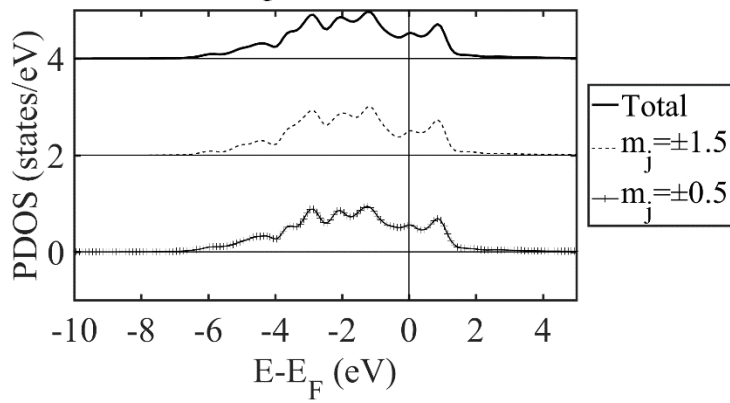
PtCo₃: Pt d j=1.5



PtCo₃: Pt d j=2.5



PtCo₃: Co d j=1.5



PtCo₃: Co d j=2.5

